Report
R-19-10
February 2019

Modelling diffusion through compacted bentonite in the BHA vault

Report for the safety evaluation SE-SFL

Andrés Idiart
Emilie Coene

SVENSK KÄRNBRÄNSLEHANTERING AB

SWEDISH NUCLEAR FUEL
AND WASTE MANAGEMENT CO

Box 3091, SE-169 03 Solna
Phone +46 8 459 84 00
skb.se

SVENSK KÄRNBRÄNSLEHANTERING

ISSN 1402-3091
SKB R-19-10
ID 1671894
February 2019

Modelling diffusion through compacted bentonite in the BHA vault

Report for the safety evaluation SE-SFL

Andrés Idiart, Emilie Coene
Amphos 21 Consulting S. L.

Summary

In this work, a set of two-dimensional models is presented that simulate the diffusion of the radionuclide $^{36}Cl^-$ across the bentonite backfill of the BHA vault in the SFL repository. The BHA vault is one of the two main vaults of the proposed repository for long-lived low and intermediate level waste in Sweden. The waste planned for disposal in SFL comprises waste from the operation and decommissioning of the Swedish nuclear power plants, waste from the early research in the Swedish nuclear programmes (legacy waste), and waste from medicine, industry and research. The focus is on the assessment of the dose of $^{36}Cl^-$ released from the waste domain and reaching the fracture system of the host rock over a time span of 1 million years. Several conceptual models of diffusion through compacted bentonite are tested. In particular, two empirical models, a semi-empirical model and two mechanistic models are used. One of the latter is based on the multi-porosity model and the other one on the single porosity Donnan equilibrium model. A base case has been formulated, conceptualized, and implemented in a two-dimensional setup for each of the above-mentioned diffusion models, based on the most plausible scenario. In addition, a number of sensitivity analyses are presented to assess the impact of chemical composition of the background electrolyte, the effective diffusion coefficient of the bentonite and the magnitude of the equivalent flow through the fractures intersecting the vault. All models presented are implemented in Comsol Multiphysics. The implications of the results and the main outcomes of the models are discussed and a comparison between different models is presented. In general, the different modelling approaches yield comparable results and predict a maximum $^{36}Cl^-$ release of $4-33 \times 10^7$ Bq/year after 1 300−9 600 years.

Sammanfattning

I detta arbete presenteras en uppsättning tvådimensionella modeller vilka simulerar diffusionen av radionukliden $^{36}Cl^-$ genom bentonitfyllningen i BHA-förvaret i SFL. BHA-förvaret är en av de två huvuddelarna av det föreslagna förvaret för långlivat låg- och medelaktivt avfall i Sverige. Avfallet som planeras för i SFL består av avfall från driften och avvecklingen av de svenska kärnkraftverken, avfall från tidig forskning i det svenska kärnkraftsprogrammet (historiskt avfall) och avfall från medicin, industri och forskning. Fokus i studien ligger på bedömningen av dosen av $^{36}Cl^-$ som frigörs från avfallsvolymen och når spricksystemet från berget över en tidsperiod på 1 miljon år. Flera konceptuella modeller av diffusion genom kompakterad bentonit har testas. Dessa utgörs av två empiriska modeller, en semi-empirisk modell och två mekanistiska modeller. En av de senare är baserad på en multiporositetsmodell och den andra på den singelporositet tillsammans med en Donnan-jämviktsmodell. Ett basfall har formulerats, konceptualiserats och implementerats i en tvådimensionell geometri för var och en av diffusionsmodellerna, baserat på det mest trovärdiga scenariot. Dessutom presenteras ett antal känslighetsanalyser för att bedöma påverkan av bakgrundselektrolytens kemiska sammansättning, den effektiva diffusionskoefficienten i bentoniten och storleken av flödet genom sprickorna korsar förvaret. Alla modeller som presenteras har implementerats i Comsol Multiphysics. Slutsatserna av analysen och de viktigaste resultaten från modellerna diskuteras och en jämförelse av olika modeller presenteras. Generellt ger de olika modelleringsmetoderna jämförbara resultat och uppskattar en maximal $^{36}Cl^-$-frigörelse av $4-33 \times 10^7$ Bq/år efter en period av 1 300−9 600 år.

Contents

1 Introduction and objectives 7

2 Scope and methodology 9
2.1 Approach 1: Multi-porosity model 10
2.2 Approach 2: Van Loon et al. (2007) 11
2.3 Approach 3: Donnan equilibrium model 11
2.4 Approach 4: Ochs and Talerico (2004) 12
2.5 Approach 5: Wersin et al. (2014) 13

3 Description of conceptual model 15
3.1 Base case 15
3.1.1 Geometry and boundary conditions 15
3.1.2 Physical properties of the barriers 16
3.2 Sensitivity cases 18
3.2.1 Background electrolyte composition 18
3.2.2 Space-dependent background electrolyte composition 19
3.2.3 Diffusion coefficient of bentonite 19
3.2.4 Equivalent fracture flow 20

4 Implementation and verification 21

5 Numerical model setup 23

6 Results 25
6.1 Base case 25
6.2 Sensitivity cases 29
6.2.1 Effect of homogeneous background electrolyte composition 29
6.2.2 Effect of space-dependent background electrolyte composition 31
6.2.3 Effect of diffusion coefficient of bentonite 32
6.2.4 Effect of equivalent fracture flow, Q_{eq} 32
6.3 Summary of results 33

7 Summary and conclusions 35

References 37

1 Introduction and objectives

SKB plans to dispose of long-lived low and intermediate level waste (LILW) in a deep geological repository, named SFL. The total capacity of SFL is estimated to approximately 16 000 m^3. About one third of the waste originates from nuclear power plants in the form of neutron-irradiated components and control rods. The remainder comes from AB SVAFO and Studsvik Nuclear AB, who manage the legacy waste and the waste from hospitals, industry and research. Possible repository concepts for SFL have been evaluated and Elfwing et al. (2013) proposed a repository concept to be analysed in an evaluation of post-closure safety (SE-SFL). This study focusses on the repository concept denoted as BHA. The main component of the engineered barrier system is a bentonite backfill that surrounds a concrete structure containing the waste.

The suitability of compacted bentonite to construct the backfill is based on its confining properties, i.e. an elevated swelling capacity, a very low permeability (minimizing or even eliminating advective transport), and a large sorption capacity for certain species. Under these conditions, solute transport in water saturated bentonite, as considered in the present study, occurs almost exclusively by diffusion. As a result, the release of radionuclides in the event of a failure of the waste containment structures is expected to be limited by the bentonite barrier.

Even though diffusion in compacted clay and bentonite has been intensively studied during the last three decades (see a recent non-exhaustive review in Idiart and Pękala 2016), there remain at present a number of controversial issues regarding a mechanistic representation of the underlying phenomena. These issues result, in most of the cases, from a lack of a well-established and widely accepted nano-/micro-structural conceptual model of compacted bentonite and clayey materials at different dry densities and salinities.

In such high density porous media, with very small pore sizes, the validity of the single porosity Fickian diffusion approach has been questioned in some cases, as it is shown to not correctly represent the diffusion of cations, anions and neutral species simultaneously. The effective diffusion coefficient is shown to be dependent on the dry density of the material, as well as on the salinity (ionic strength) of the external solution. Experiments show that the transport of cations at steady-state is faster than that of neutral species and in turn the transport of anions is slower than the rest of species. This behaviour is typically explained in terms of distinct tortuosity factors for cations, anions, and neutral species due to overlapping of electrical double layers of clay minerals at high degrees of compaction. The increased diffusivity of cations is sometimes also explained in terms of "surface diffusion". Therefore, more complex mechanistic models have been proposed in the literature to try to capture experimental observations.

In this study, different available approaches and models are used to estimate the flux of $^{36}Cl^-$ that can escape the BHA vault by diffusion across the bentonite backfill. Previous efforts to assess the impact of different diffusion models on the fluxes of Cl^- have been presented in Idiart and Pękala (2016). Their results showed that the fluxes in a simple 1D setup are comparable between the different models (best guesses differed by less than a factor of 6), which is a consequence of the similarity between the different effective diffusion coefficients. These differences are assessed in the present work using a setup that is more suitable for the BHA vault concept.

The main objective of the present study is to predict the long-term (i.e. 1 million years) behaviour of $^{36}Cl^-$ under repository conditions and quantify its release from the waste domain towards the fractured host rock. Emphasis is on the diffusion resistance of the bentonite backfill, which is considered the main barrier for radionuclide transport. The models consider relevant parameterization of the engineered barrier in terms of dimensions, physical properties (porosity, dry density, diffusivity), and chemical environment.

2 Scope and methodology

The methodology to estimate the release of $^{36}Cl^-$ from the BHA vault over time is based on the implementation in the finite element software Comsol Multiphysics version 5.3 (COMSOL 2017) of a set of diffusion models through the compacted bentonite of the backfill. A quantitative inter-comparison of the selected diffusion approaches is performed over a single geometrical and physical model of the waste-backfill-fractured host rock system. Transient conditions are considered due to the dependence of the source term with time, i.e. the release of $^{36}Cl^-$ leads to a decrease in its concentration at the source.

A two-dimensional representation of the BHA vault cross-section is considered. Bentonite is assumed to be water saturated and advective flow is not taken into account (once saturated, solute transport in the bentonite buffer is typically considered to be diffusion-driven). Isothermal conditions are considered, with a constant temperature of 15 °C, as expected under SFL repository conditions (SKB 2019). This temperature is used to correct the diffusion coefficient of one of the models (Wersin et al. 2014) and for the geochemical calculations of the background chemical conditions performed in Phreeqc (Parkhurst and Appelo 2013). Radioactive decay of $^{36}Cl^-$ is included in all the models.

A base case is proposed, conceptualized and implemented based on the most plausible scenario according to up-to-date knowledge of the system (geometry, physical properties of the barriers, geochemical conditions, etc.). This base case is simulated using five different diffusion models, as listed in Table 2-1. Given the relatively high level of uncertainty in some of the parameters and variables that control the system, a set of sensitivity analyses is proposed to assess the impact on the results.

Table 2-1. Approaches considered for modelling of ^{36}Cl diffusion in MX-80 compacted bentonite.

Approach n°	Description	Reference
1	Multi-porosity (free, EDL and IL)	Appelo (2013)
2	Semi-empirical	Van Loon et al. (2007)
3	Single porosity, Donnan equilibrium	Birgersson and Karnland (2009)
4	Empirical	Ochs and Talerico (2004)
5	Empirical	Wersin et al. (2014)

EDL = electrical double layer porosity; IL = interlayer porosity.

The main differences between the different approaches lie in the porosity types they take into account and, as a result, the effective diffusion coefficients and available porosities they consider for anions. The total or physical porosity (ϕ_{tot}) of compacted bentonite can be calculated from the following expression:

$$\phi_{tot} = 1 - \frac{\rho_d}{\rho_s} \qquad \text{Equation 2-1}$$

where ρ_d is the dry density ($kg \cdot m^{-3}$), i.e. the mass of clay (without hydration water) per unit total volume, and ρ_s ($kg \cdot m^{-3}$) is the montmorillonite crystal density (grain density).

Several authors have proposed to distribute this total porosity into 2 and even 3 types of water/porosities in compacted bentonite to model ionic transport in bentonite (e.g. Bourg et al. 2003, Wersin 2003, Wersin et al. 2004, Muurinen et al. 2007). Bradbury and Baeyens (2003), for instance, suggested three different types of water in bentonite pores: free pore water, interlayer water (IL) and electrical double layer (EDL) water.

The free pore water consists of a charge balanced aqueous solution of cations and anions. Interlayer water is found between montmorillonite layers and contains water, cations and a reduced amount of anions, compensating the structural charge deficit of montmorillonite layers. EDL water, on the other hand, is present between the mineral surface and the free water. It contains cations and a small concentration of anions. The excess of cations balances the remaining charge at the outer surface of the montmorillonite. The proportion of each type of water depends on the degree of compaction of bentonite (dry density), the salinity of the solution, or the amount of accessory minerals.

However, in all the approaches solute transport through the bentonite backfill occurs according to the following expression:

$$\phi_{av,i}\,\frac{\partial c_i}{\partial t} = \nabla(D_e \nabla c_i) - \phi_{av,i}\lambda_i c_i \qquad \text{Equation 2-2}$$

in which c_i is the concentration of the ionic species i, $\phi_{av,i}$ is the diffusion available porosity of species i, λ_i is its radioactive decay constant (s^{-1}) and the effective diffusion coefficient, $D_{e,i}$ (m^2/s), is defined in the following way:

$$D_{e,i} = \phi_{av,i} \cdot \tau \cdot D_{w,i} \qquad \text{Equation 2-3}$$

where $D_{w,i}$ (m^2/s) is the diffusion coefficient of species i in free solution (or self-diffusion coefficient) and τ (-) is the overall tortuosity of the porous system ($0<\tau<1$).

The methodology used in each approach to obtain the effective diffusion coefficient and the available porosity, and to define their boundary conditions is explained below.

2.1 Approach 1: Multi-porosity model

Approach 1 (Appelo 2013) considers all three porosity types: interlayer, EDL and free. It is assumed, however, that the interlayer water is devoid of anions and therefore that $^{36}Cl^-$ is not transported through it. $^{36}Cl^-$, then, is transported only in the free and EDL porewaters, following Equations 2-4 and 2-5, respectively:

$$\phi_f\,\frac{\partial c_{i,f}}{\partial t} - \phi_f\,\frac{\delta}{\theta^2}\,D_{w,i}\,\nabla^2 c_{i,f} = -\phi_f\,\lambda_i\,c_{i,f} \qquad \text{Equation 2-4}$$

$$\phi_{EDL}\,\frac{\partial c_{i,EDL}}{\partial t} - \phi_{EDL}\,\frac{\delta}{\theta^2} D_{w,i}\,\nabla^2 c_{i,EDL} = -\phi_{EDL}\,\lambda_i\,c_{i,EDL} \qquad \text{Equation 2-5}$$

where ϕ_f and ϕ_{EDL} are the free and EDL porosities, respectively, $c_{i,f}$ and $c_{i,EDL}$ the concentration of a species i in each porosity type, and $\frac{\delta}{\theta^2}$ the tortuosity-constrictivity factor of the pores. We define the Cl^- concentration ratio between EDL and free water, r, and the average concentration, c_{av}, as:

$$r = \frac{c_{i,EDL}}{c_{i,f}} \qquad \text{Equation 2-6}$$

$$c_{i,av} = c_{i,f}\,\frac{\phi_f + r\cdot\phi_{EDL}}{\phi_f + \phi_{EDL}} \qquad \text{Equation 2-7}$$

By adding up transport Equations 2-4 and 2-5 and performing some algebra, we obtain one single transport equation in terms of the average concentration in EDL and free porewaters:

$$(\phi_f + \phi_{EDL})\,\frac{\partial c_{i,av}}{\partial t} - (\phi_f + \phi_{EDL})\,\frac{\delta}{\theta^2}\,D_{w,i}\,\nabla^2\,c_{i,av} = -(\phi_f + \phi_{EDL})\lambda_i\,c_{i,av} \qquad \text{Equation 2-8}$$

Note that for this approach, the total porosity of the bentonite needs to be distributed between the three porosity types. The interlayer porosity (ϕ_{IL}) can be calculated by means of the following expression (e.g. Appelo 2013):

$$\phi_{IL} = V_{IL} \cdot f_{dens} \cdot w_{mm} \cdot \rho_{dry} \qquad \text{Equation 2-9}$$

where w_{mm} (-) is the montmorillonite weight fraction, f_{dens} (-) is the water density ratio between the interlayer and free porosity, and the volume of the interlayer (V_{IL}, m^3/kg) can be calculated as (e.g. Appelo 2013):

$$V_{IL} = \frac{t_{IL}\cdot A_{planar,int}}{2} \qquad \text{Equation 2-10}$$

The internal planar surface, $A_{planar,int}$ (m^2/kg), and the interlayer thickness, t_{IL} (m), may be calculated as (Muurinen et al. 2007, Appelo 2013):

$$A_{planar,int} = 2 \cdot \frac{a\cdot b\cdot(n_c-1)}{n_c} \cdot \frac{N_A}{M_w} \qquad \text{Equation 2-11}$$

$$t_{IL} = 1.41 \cdot 10^{-9}[\mathrm{m}] - 4.9 \cdot 10^{-13}\left[\frac{m^4}{kg}\right] \cdot \rho_{dry}\left[\frac{kg}{m^3}\right] \qquad \text{Equation 2-12}$$

where N_A is the Avogadro number, i.e. 6.02×10^{23}, M_w is the molecular weight, a and b are the dimensions of the monoclinic unit cell in the horizontal plane, and n_c is the stacking number of TOT (Tetrahedral-Octahedral-Tetrahedral) montmorillonite layers.

In turn, the thickness of the EDL depends on the ionic strength of the pore solution, so that its volume can be calculated from the external surface area of charged mineral, A_{ext} ($m^2/kg_{dry\ bentonite}$), multiplied by the double layer thickness, t_{EDL} (m):

$$\phi_{EDL} = A_{ext} \cdot w_{mm} \cdot \rho_{dry} \cdot t_{EDL} \qquad \text{Equation 2-13}$$

The double layer thickness can be approximated by the Debye length κ^{-1} multiplied by a constant λ:

$$t_{EDL} \cong \lambda \cdot \kappa^{-1} = \lambda \cdot \sqrt{\frac{3.94 \cdot 10^{-24} \cdot \varepsilon_r \cdot T}{I}} \qquad \text{Equation 2-14}$$

In the previous expression, I (mol/kgw) stands for the ionic strength of the pore solution, T is temperature (in Kelvin), ε_r (-) is the relative dielectric constant of water, and the λ multiplier (-) represents the number of Debye lengths across the double layer thickness.

Free porosity, finally, can be calculated provided that the EDL and IL contributions to total porosity are known:

$$\phi_f = \phi_{tot} - (\phi_{EDL} + \phi_{IL}) \qquad \text{Equation 2-15}$$

Obviously, these equations are valid as long as the sum of interlayer and double layer porosities is smaller than the total porosity, which is not always the case (Idiart and Pękala 2016). In this work, Approach 1 is only used in the cases where a positive free porosity can be calculated using the above formulation.

2.2 Approach 2: Van Loon et al. (2007)

Van Loon et al. (2007) studied the diffusion of $^{36}Cl^-$ in compacted bentonite using through-diffusion, out-diffusion and profile analysis techniques. Experiments were carried out on bentonite samples of varying dry density (1 300–1 900 kg/m^3) and ionic strength (0.01 – 1.00 M). Based on their experimental results, they identified and estimated two critical parameters: chloride accessible porosity and effective diffusion coefficient.

Note that this model does not consider different porosity types, but summarizes the presence (or absence) of chloride in each of them by means of a single, accessible porosity. The chloride accessible porosity was fitted to an exponential expression that depends on the ionic strength of the external solution, I, in the following way:

$$\phi_{av,Cl} = \phi_{av,Cl}^{max} - A \cdot e^{-B \cdot I} \qquad \text{Equation 2-16}$$

where A and B are fitting coefficients, and $\phi_{av,Cl}^{max}$ is identified as the inter-particle pore space. The values of these parameters that were obtained for a dry density of 1 600 kg/m^3 are 0.092, −2.40 and 0.098, respectively. Using a collection of previously published data, the authors fitted the effective diffusion coefficient to the following empirical formula (analogous to Archie's law):

$$D_{e,Cl} = D_{w,Cl} \cdot \phi_{av,Cl}^{n} \qquad \text{Equation 2-17}$$

where $D_{w,Cl}$ is the free water diffusion coefficient and n is an empirical coefficient equal to 1.9 ± 0.1. Using the two above formulae, the diffusive flux of Cl^- in compacted bentonite can be calculated as a function of the ionic strength of the pore water.

2.3 Approach 3: Donnan equilibrium model

Approach 3 is based on the model proposed by Birgersson and Karnland (2009). This model considers solute diffusion through a single interlayer porosity, which corresponds to water present between montmorillonite sheets. The interlayer water has a net positive charge that compensates the negatively

charged montmorillonite surface. As a result, there is a concentration discontinuity at the clay/external solution interface (drop of anion concentration and increase in cation concentration) that causes a lower anion diffusive flux through the bentonite.

The formulation of the Donnan equilibrium model is derived from thermodynamics, i.e. from chemical potentials of the interlayer (μ_i^{int}) and external (μ_i^{ext}) solutions:

$$\mu_i^{int} = \mu_{0,i} + RT \cdot ln\left(a_i^{int}\right) + F \cdot z_i \cdot \Delta\varphi \qquad \text{Equation 2-18}$$

$$\mu_i^{ext} = \mu_{0,i} + RT \cdot ln\left(a_i^{ext}\right) \qquad \text{Equation 2-19}$$

where a_i^{int} and a_i^{ext} are the activities of ion i in the internal and external solutions respectively, z_i the charge of that species, F the Faraday constant, and $\Delta\varphi$ the mean Donnan potential in the interlayer water. The ion activity is defined as:

$$a_i = \gamma_i c_i \qquad \text{Equation 2-20}$$

where γ_i and c_i are the activity coefficient and aqueous concentration of a given species, respectively. At equilibrium, the chemical potentials given in Equations 2-18 and 2-19 are equal and therefore:

$$\frac{a_i^{int}}{a_i^{ext}} = exp\left(-\frac{F \cdot z_i \cdot \Delta\varphi}{RT}\right) = \Xi^{-z_i} \qquad \text{Equation 2-21}$$

Ξ being the ion equilibrium coefficient. An additional constraint is added in order to fulfil charge balance in the interlayer:

$$\sum \Xi^{-z_i} \cdot c_i^{ext} \cdot z_i = \frac{CEC \cdot \rho_w}{w \cdot (1\frac{eq}{mol})} \qquad \text{Equation 2-22}$$

c_i^{ext} (mol/kgw) is the ion i concentration in external solution, CEC (eq/kg dry clay) the cation exchange capacity of the clay, ρ_w (kg/m^3) the water density, and w (kg$_w$/kg dry clay) the water content in the clay.

The previous equations have been used to calculate the $^{36}Cl^-$ concentration drop at the concrete – bentonite interface, that is, the boundary condition for $^{36}Cl^-$ transport from the cementitious waste domain towards the bentonite backfill.

In this approach, only an interlayer porosity is assumed and thus $\phi_{IL} = \phi_{tot}$. With this model the total porosity is accessible to chloride, while anion fluxes are reduced due to the concentration drop between the external groundwater and the bentonite barrier. In Birgersson and Karnland (2009), the effective diffusion coefficient is defined as:

$$D_e = \phi_{IL} \cdot D_c \qquad \text{Equation 2-23}$$

where D_c (m^2/s) is the pore diffusion coefficient. Fitting of experimental data from different bentonites with ρ_{dry} = 1 600 kg/m^3 yielded a value of $D_c = 1.26 \times 10^{-10}$ m^2/s (Birgersson and Karnland 2009).

2.4 Approach 4: Ochs and Talerico (2004)

Ochs and Talerico (2004) presented an assessment and recommendation of key transport parameter values (diffusion-available porosity, effective diffusivity and distribution coefficient) for a total of 38 elements. These values were obtained from a systematic review of available datasets in the literature and/or from thermodynamic models and were derived for conditions relevant to the prospective disposal, e.g. for a specific pore water composition, solid/water ratio and dry density of the MX-80 bentonite at repository conditions. The majority of these recommended values were later used to predict the transport of radionuclides in compacted bentonite in the SR-Can (SKB 2006) and SR-Site (SKB 2010) Performances Assessments.

The recommended values of effective diffusion coefficient and available porosity for chloride are 1.0×10^{-11} m^2/s and 0.17, respectively. Note that the limited number of diffusion data sets did not allow estimating these parameters as a function of variable conditions such as porewater salinity. They are considered to be a realistic estimate for groundwaters of intermediate to high salinity, i.e. 0.2 to 1 M (Ochs and Talerico 2004). Similarly to approach 2 (Van Loon et al. 2007), the effect of the different porosity types is approximated by means of the accessible porosity parameter.

2.5 Approach 5: Wersin et al. (2014)

Wersin et al. (2014) compiled currently available data on anion, cation and neutral species diffusion in compacted bentonite. They derived the following empirical expression for the effective diffusion coefficient of anions (D_e) in compacted bentonite at 25 °C as a function of the bentonite dry density (ρ_d) and ionic strength (I):

$$D_e(25°C) = 3 \cdot 10^{-7} \cdot e^{-0.0066 \cdot \rho_d} \cdot I^{0.64(\pm 0.08)} \quad \text{Equation 2-24}$$

A dependence of the diffusion coefficient on temperature is also considered by Wersin et al. (2014) and is used here to obtain the effective diffusion coefficient at 15 °C:

$$D_e(T) = D_e(0°C) \cdot e^{0.026 \cdot T} \quad \text{Equation 2-25}$$

In this approach, it is assumed that both the interlayer and double layer porosities are devoid of anions (Wersin et al. 2014). This approximation may cause the model to under-predict $^{36}Cl^-$ fluxes, but this effect should be small given that these porosities present low anion concentrations. The anion accessible porosity can thus be obtained with the following expression:

$$\phi_{acc} = \phi_{tot} - \phi_{IL} - \phi_{EDL} \quad \text{Equation 2-26}$$

where they use the interlayer porosity calculated for MX-80 bentonite in Appelo (2013), ϕ_{IL} = 0.212. The EDL porosity is calculated as follows:

$$\phi_{EDL} = d_a \frac{A_{mm}\, m_{mm}}{p} \quad \text{Equation 2-27}$$

$$d_a = a \cdot \kappa^{-1} = a \cdot \frac{3.037 \cdot 10^{-10}}{\sqrt{I}} \quad \text{Equation 2-28}$$

where d_a (m) is the anion exclusion distance at the external surface, A_{mm} (m^2/g montmorillonite) the total surface of montmorillonite, m_{mm} (kg/L bentonite) the mass of montmorillonite, p (-) the stacking number of montmorillonite layers, κ (m) the Debye length and a is a factor that depends on the ionic strength. Tournassat (2008) proposed a value of a = 1.9 for ionic strengths below 0.05, a = 1.2 for ionic strengths greater than 0.1, and a linear interpolation for values in between.

3 Description of conceptual model

3.1 Base case

3.1.1 Geometry and boundary conditions

A cross-sectional view of the BHA vault is shown in Figure 3-1 (SKB 2019). The 2D model considered in this work represents a horizontal cross-section across the vault at mid-height of the waste domain, see Figure 3-1 and Figure 3-2.

As displayed in Figure 3-2, the BHA vault is assumed to be intersected perpendicularly to its axis by fractures in the host rock with a spacing of 30 m. Given that the length of the tunnel is 170 m (SKB 2019), a total of 6 fractures is considered to intersect the vault. With this setup, the length of the vault can be divided into 15 m-thick sections with a vertical symmetry plane at each side: the mid-plane of a fracture and the mid-distance between fractures, both perpendicular to the vault axis. The fracture width is assumed to be 1 mm, as this value is large enough to consider a fixed concentration as a realistic boundary condition. The 2D model used in this work studies a plane that crosses the vault horizontally. A third vertical symmetry plane is considered along the vault axis.

The 2D models developed here conceptualize the fractured rock in a simplified way as a set of discrete fractures with intact rock in between, similar to Wessely and Shahkarami (2019). This approach sets the focus on diffusion through bentonite, as $^{36}Cl^-$ has to diffuse towards the fractures, which constitutes a longer diffusion path than when considering an equivalent porous medium. Although different conceptualizations of the fractured rock may yield different results in terms of $^{36}Cl^-$ release, the goal of this study is to compare different diffusion models using otherwise a similar setup. In this context, fractures are assumed to have a high transport capacity, the fractures intersecting the vault are assumed as perfect $^{36}Cl^-$ sinks in the base case, with a fixed concentration equal to zero. On the other hand, the intact rock is assumed to have a negligibly small diffusion coefficient and is considered in the model as a no flow boundary condition. The remaining boundaries of the system consist of no flow boundary conditions, as they represent the symmetry planes at the centre of the waste, the mid-aperture of the fracture, and the mid-distance between two fractures.

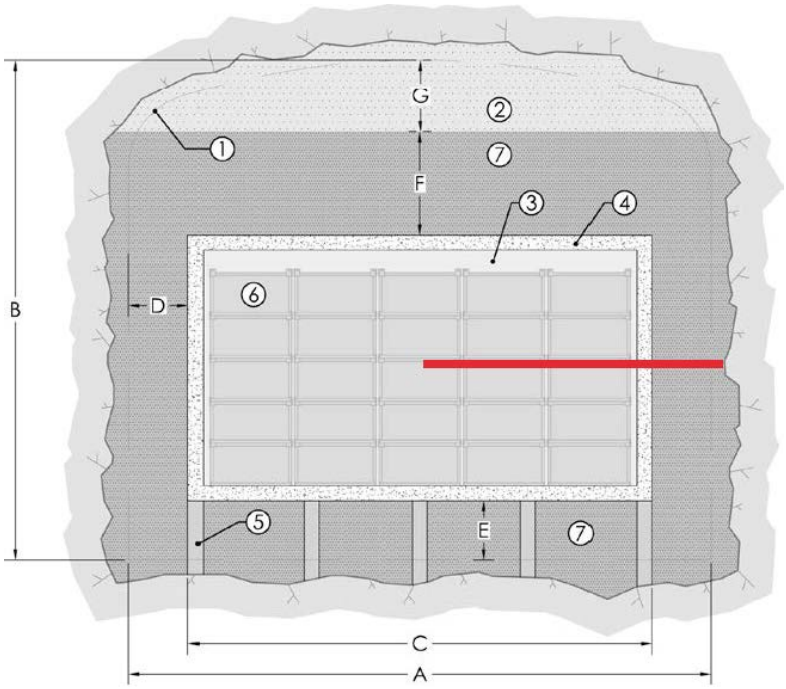

Figure 3-1. *Position of the 2D studied domain (in red) referred to the 2D cross-sectional view of the BHA vault. Legend: 1) Theoretical tunnel contour. 2) Bentonite pellets. 3) Grout. 4) Concrete structure for the operating period (0.5 meter). 5) Granite pillars. 6) Waste containers. 7) Bentonite blocks. Approximate dimensions: A = 20.6 m, B = 18.5 m, C = 16 m, D = 2.3 m, E = 2.4 m, F = 4 m, G = 3.7 m. Adapted from SKB (2019).*

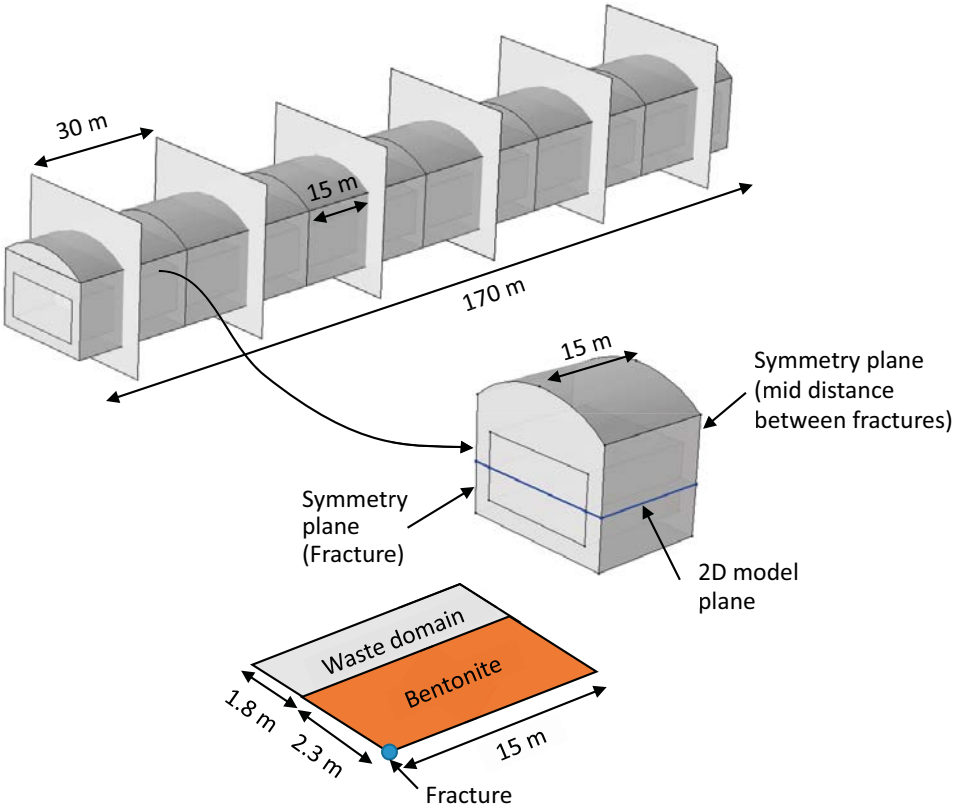

Figure 3-2. *Top: sketch of the BHA vault with fractures perpendicular to its axis with a spacing of 30 m and detail of the 3D domain considered in the conceptual model. Bottom: detail of the 2D plane considered in the simulations and its dimensions in metres.*

The thickness of the bentonite backfill in the 2D model is of 2.3 m, in accordance with the vault dimensions given in SKB (2019), see Figure 3-2. On the other hand, the dimension of the waste domain is calculated from the assumption that the waste-to-backfill volume ratio in the model is the same as that given in SKB (2019). From the dimensions in Figure 3-1, the volume (per meter depth) of bentonite backfill is 170.48 m^3 (disregarding the contribution of bentonite pellets), while the volume of waste domain is 134.4 m^3. Thus, the waste-to-backfill volume ratio is 0.79. In the 2D model, this is equivalent to a waste domain thickness of 1.813 m.

This 2D geometry setup ensures a correct amount of total $^{36}Cl^-$ in the system, but is conservative when it comes to its release. Those is, a Bentonite thickness of 2.3 m is used, which corresponds to the lateral walls, but the bentonite layers on top and at the bottom of the vault are 4 and 2.4 m respectively, such that the 2D simplification used here over-estimates $^{36}Cl^-$ release.

3.1.2 Physical properties of the barriers

Transient diffusion of $^{36}Cl^-$ from the waste towards the fractured rock is calculated with Equation 2-2, assuming water saturated conditions and no sorption on the solid phase. In this equation, a $^{36}Cl^-$ radioactive decay constant of 7.30×10^{-14} s^{-1} is used, corresponding to a half-life of 301 000 years (e.g. Wessely and Shahkarami 2019). All simulations consider isothermal conditions with a temperature of 15 °C, as expected under SFL repository conditions (SKB 2019).

The available porosity in the waste domain is 0.31, as calculated from geometrical considerations (SKB 2019). The effective diffusion coefficient in this domain is set to a high value (10^{-9} m^2/s) such that $^{36}Cl^-$ transport across the backfill is not limited by diffusion in the waste domain.

The bentonite available porosity and effective diffusion coefficient are calculated for each approach with the formulations outlined in Chapter 2 and using the parameter values given in Table 3-1 to Table 3-5. The bentonite dry density and montmorillonite grain density are 1 577 kg/m^3 and 2 732 kg/m^3, respectively (SKB 2011), which results in a total porosity of 0.423 (Equation 2-1).

Table 3-1. Parameters used in the multi-porosity model (Approach 1).

Parameter	Symbol	Value	Unit
[1]Montmorillonite crystal unit-cell dimension	a	5.23×10^{-10}	m
[1]Montmorillonite crystal unit-cell dimension	b	9.05×10^{-10}	m
[1]Montmorillonite crystal unit-cell dimension	c	9.60×10^{-10}	m
[1]Stacking number in the a-direction	n_a	200	–
[1]Stacking number in the b-direction	n_b	200	–
[2]Stacking number in the c-direction	n_c	5	–
[3]Molecular weight	M_w	0.735	kg/mol
[4]Montmorillonite weight fraction	w_{mm}	0.84	–
[4]Cation exchange capacity	CEC	0.75	eq/kg dry bentonite
[1]Density ratio of interlayer water	f_{dens}	1	–
[5]Montmorillonite total surface area	A_{tot}	800	m^2/g dry bentonite
[5]Montmorillonite external surface area	A_{ext}	30	m^2/g dry bentonite
[3]N° of Debye lengths in double layer	λ	2	–
[3]Tortuosity-constrictivity factor	δ/θ^2	0.1	–
[6]Free water diffusion coefficient	D_w	2.03×10^{-9}	m^2/s
Cl^- concentration ratio in eq. 2.6	r	0.180	–

[1] Appelo (2013); [2] Pusch (2001); [3] Idiart and Pękala (2016); [4] SKB (2011); [5] Idiart et al. (2019); [6] Appelo and Postma (2005).

Table 3-2. Parameter values used in Approach 2, obtained by Van Loon et al. (2007).

Parameter	Symbol	Value	Unit
Fitting parameter, Equation 2-16	A	0.092	–
Fitting parameter, Equation 2-16	B	−2.40	–
Inter-particle pore space	$\phi_{av,Cl}^{max}$	0.098	–
Fitting parameter, Equation 2-17	2	1.9	–

Table 3-3. Parameter values used in the Donnan equilibrium model (Approach 3).

Parameter	Symbol	Value	Unit
[1]Pore diffusion coefficient	D_c	1.26×10^{-10}	m^2/s
Chloride available porosity	$\phi_{av,Cl}$	0.423	–
[2]Cation exchange capacity	CEC	0.75	eq/ kg dry bentonite
[2]Water content in clay	w	0.27	kg_w/kg dry clay
Water density	ρ_w	1 000	kg/m^3
Ion equilibrium coefficient	Ξ	0.0633	–

[1] Birgersson and Karnland (2009); [2] SKB (2011).

Table 3-4. Parameter values used in Approach 4, from Ochs and Talerico (2004).

Parameter	Symbol	Value	Unit
Chloride effective diffusion coefficient	$D_{e,Cl}$	1.0×10^{-11}	m^2/s
Chloride available porosity	$\phi_{av,Cl}$	0.17	–

Table 3-5. Parameter values used in Approach 5. Fitted by Wersin et al. (2014) with the approach of Appelo (2013) based on anion accessible porosities measured as a function of montmorillonite density.

Parameter	Symbol	Value	Unit
Stacking number	p	4.8	–
Montmorillonite surface area	A_{mm}	487	m^2/g dry bentonite
Montmorillonite mass	m_{mm}	1.37	kg/l

Table 3-6. Concrete and bentonite porewater compositions at 15 °C obtained in Idiart et al. (2019), and used here as the base case porewater compositions in the waste and bentonite domains, respectively.

	Concrete porewater	Bentonite porewater
pH	12.83	7.19
Temperature (°C)	15	15
Ionic strength (M)	0.066	0.227
Species (totals, in M)		
Al	5.54E−07	4.11E−10
C	1.00E−05	2.70E−03
Ca	2.43E−02	1.85E−02
Cl	5.55E−05	1.38E−01
K	7.60E−05	1.14E−03
Mg	2.53E−08	8.86E−03
Na	4.79E−03	1.57E−01
S(6)	3.29E−03	3.60E−02
Si	4.52E−05	1.34E−04

From Table 3-1, it follows that 3.75 % of the montmorillonite surface area is external and is used to calculate EDL porosity. The CEC of the EDL porewater is 0.028 eq/g dry bentonite, or 0.275 eq/l EDL+ free porewater (ρ_D = 1 577 kg/m^3 and $\phi_f + \phi_{EDL}$ = 0.16). The CEC of the EDL, the bentonite porewater composition and its ionic strength at 15 °C (Table 3-6), have been used to calculate the Cl^- concentration ratio, *r*, used in the multi-porosity model with Phreeqc, as given in Table 3-1.

The initial $^{36}Cl^-$ concentration in the bentonite backfill is 0 mol/m^3. The initial concentrations of different radionuclides in the waste and concrete of the BHA vault can be calculated from the inventory of the waste given in SKB (2019). The value obtained for $^{36}Cl^-$, used here as the initial condition of the waste domain, is 0.13 mol/m^3 water. This value is used, as is, in approaches 2, 4 and 5. In approach 1, however, this value corresponds to the concentration in the free porewater of bentonite at its boundary, while the variable solved for is the average concentration (see Section 2.1). The initial average concentration in the waste can be calculated with Equation 2-7.

In approach 3, on the other hand, the $^{36}Cl^-$ concentration in the waste corresponds to the external concentration, i.e. outside the bentonite domain, while the transport equation is solved in terms of interlayer concentration (Section 2.3). In order to calculate the interlayer concentration in equilibrium with the initial waste porewater solution, the ion equilibrium coefficient must be obtained by solving Equations 2-21 and 2-22 for each of the aqueous species. This study considers a cementitious waste porewater in equilibrium with portlandite. The composition of concrete porewater at 15 °C, obtained in Idiart et al. (2019), is presented in Table 3-6. The concentrations and activity coefficients of the aqueous species in concrete porewater were calculated with Phreeqc using the parameter values listed in Table 3-3, and it is assumed that, as a first approximation, the activity coefficient in the external and interlayer pore solutions are the same for a given species. The resulting ion equilibrium coefficient is 0.0633.

3.2 Sensitivity cases

3.2.1 Background electrolyte composition

The base case simulations use the bentonite porewater composition depicted in Table 3-6 as the background chemistry for diffusion of $^{36}Cl^-$ through bentonite (see Idiart et al. 2019). A set of sensitivity cases is implemented to study the impact of different porewater compositions as background electrolytes, as detailed in Table 3-7. A wide range of ionic strength is used to evaluate the sensitivity of the different models to this parameter. In particular, approaches 1, 2, and 5 are used in this sensitivity study.

Approach 3, corresponding to the Donnan equilibrium model, is also dependent on ionic strength, but in this case, it is the composition of the 'external solution' that is important. In the present study, the external solution is the waste porewater composition, which is expected to be controlled by the solubility of portlandite (Idiart et al. 2019). The ionic strength of the bentonite porewater in this approach is assumed to remain approximately constant, as determined from the CEC (Table 3-1), defining the charge that needs to be compensated by ions in the interlayer water.

The empirical data used in approach 4 (Ochs and Talerico 2004) are considered suitable for groundwaters of intermediate to high salinity (0.2–1.0 M), which is not the case of the porewaters used here. Therefore, approaches 3 and 4 are not included in this sensitivity case.

Furthermore, the low ionic strength of the old meteoric as well as the glacial end-members yield negative values of free porosity in the multi-porosity model (approach 1, see Section 2.1), and of accessible porosity in the model proposed by Wersin et al. (2014) (approach 5, see Section 2.5). Therefore, the sensitivity analysis of approaches 1 and 5 is limited to the saline end member. The calculation of the Cl^- concentration ratio between EDL and free porosities, used in the multi-porosity model, follows the same methodology as for the base case, yielding a value of $r = 0.371$ for the saline porewater. Finally, Approach 2 was simulated with all three porewaters given in Table 3-7.

Table 3-7. Groundwater compositions corresponding to the old meteoric end member (Pękala et al. 2015) and saline and glacial end members (adapted from Gimeno et al. 2010).

	Old Meteoric	Saline	Glacial
pH	8.64	8	5.8
Ionic strength (M)	0.006	1.628	5.00E−05
Species (totals)	**Concentration (M)**		
Al	1.21E−06	−	−
Br	−	4.05E−03	−
C	6.91E−04	−	2.00E−06
Ca	5.26E−04	4.82E−01	4.50E−06
Cl	4.54E−03	1.319	2.54E−05
K	7.60E−05	1.16E−03	1.00E−05
Mg	1.48E−04	8.72E−05	4.10E−06
Na	4.79E−03	3.70E−01	7.40E−06
S(VI)	3.73E−04	5.46E−03	5.20E−06
Si	1.42E−04	1.03E−04	−

3.2.2 Space-dependent background electrolyte composition

This sensitivity case consists in using a more realistic, space-dependent porewater composition in the bentonite backfill, rather than a uniform composition as in previous sections. To obtain the ionic strength distribution across the modelled bentonite domain, a simple reactive transport model with no mineral reactions was simulated with iCP (Nardi et al. 2014), coupling Comsol Multiphysics and Phreeqc. The concrete porewater composition (Table 3-6) is imposed in the bentonite-waste interface, while the old meteoric groundwater composition (Table 3-7) is fixed in the fracture-bentonite interface. The resulting steady-state ionic strength distribution within the bentonite domain is shown in Figure 3-3. As can be observed, the resulting ionic strength distribution has a minimum value of 6×10^{-3} M at the interface with the fracture. With this ionic strength, approaches 1 and 5 yield negative porosities (see discussion in Section 3.2.1). Therefore, this sensitivity case is limited to approach 2.

3.2.3 Diffusion coefficient of bentonite

The sensitivity of the different models to changes in the effective diffusion coefficient of the bentonite domain was assessed by increasing and decreasing the base case value by a factor of 10. This analysis was carried out for all approaches in order to determine if there are approaches that are more sensitive than others in terms of peak chloride fluxes to changes in the diffusion coefficient.

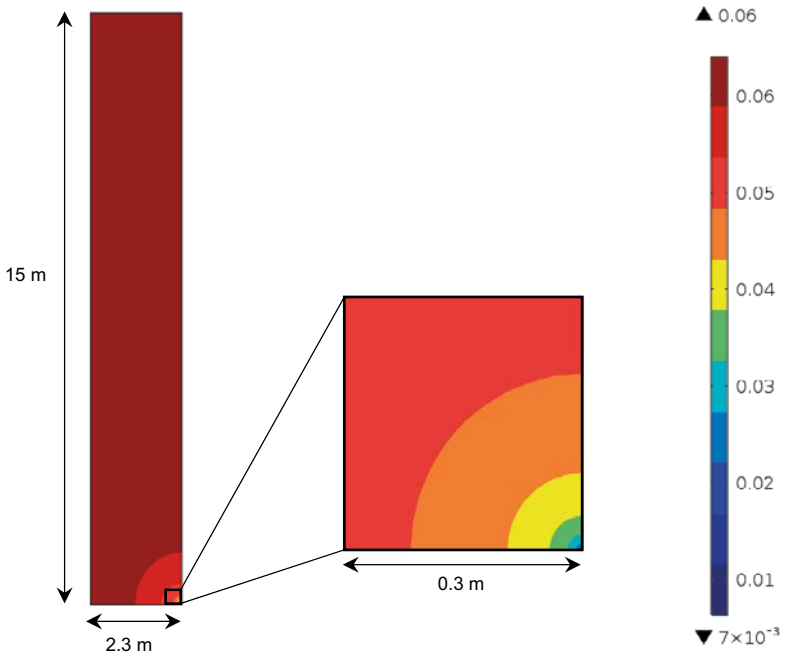

Figure 3-3. *Steady-state ionic strength distribution in the bentonite backfill, as obtained with a reactive transport model, using a concrete porewater composition at the waste-bentonite interface (left boundary), and an old meteoric groundwater composition in the fracture (bottom-right corner).*

3.2.4 Equivalent fracture flow

In all previous cases, the fractures were assumed to be perfect sinks, with a fixes $^{36}Cl^-$ concentration equal to 0. In this sensitivity case, the fractures are modelled with the classical equivalent flow concept instead, see e.g. Hartley et al. (2006). This sensitivity case was run with approaches 2, 4 and 5.

The radionuclide mass flux per square meter of surface area between the fractures and the bentonite, N_{36Cl}, in mol · m^{-2} · s^{-1}, is given by:

$$N_{36Cl} = q_{eq} \cdot (c_b - c_f) \qquad \text{Equation 3-1}$$

where q_{eq} (m^3 · m^{-2} · s^{-1}) is the equivalent fracture flowrate per unit area, and c_b and c_f the $^{36}Cl^-$ concentrations (mol/m^3) at the bentonite-fracture interface and in the fracture (assumed here to be 0), respectively. The value of q_{eq} can be calculated with the following expression:

$$q_{eq} = \frac{Q_{eq,tot}}{n_f \cdot L \cdot a} \qquad \text{Equation 3-2}$$

where $Q_{eq,tot}$ is the total equivalent fracture flowrate (m^3 · s^{-1}), n_f (-) the number of fractures, L (m) the length of the fracture – bentonite intersection and a (m) the fracture aperture. The value used in this work for the $Q_{eq,tot}$ of the BHA vault is 0.187 m^3/year, after Wessely and Shahkarami (2019). As outlined in Section 3.1, the conceptual model considers a total of 6 fractures intersecting the vault with an aperture of 1 mm. The length of the fracture-bentonite intersection, L, is equal to the outer perimeter of the bentonite blocks in Figure 3-1, i.e. 70.8 m.

4 Implementation and verification

As stated above, the different approaches described in Chapter 2 have been implemented in Comsol Multiphysics version 5.3 (COMSOL 2017). To this end, the *Transport of Diluted Species in Porous Media* built-in physics of Comsol has been adapted to each modelled approach by specifying the effective diffusion coefficient and available porosity in the *Porous Media Transport Properties* node. As stated in Chapter 2, no advective mass transfer is considered. Furthermore, the radioactive decay is implemented using a *Reactions* node.

Verification of the implementation of each approach is based on the comparison between the results obtained with the current transient Comsol models (when reaching steady-state conditions) and the results of the bentonite buffer steady-state simulations presented in Idiart and Pękala (2016), see Table 4-1. In order to obtain equivalent models to those of Idiart and Pękala (2016), the different approaches were implemented without considering radioactive decay, a fixed $^{36}Cl^-$ concentration gradient, Donnan ion equilibrium coefficients given in Idiart and Pękala (2016), and the parameters given in Table 4-2. All other parameters are the same as for the Base Case setup of this study, see Chapter 3.

Table 4-1. Results obtained in Idiart and Pękala (2016) on steady-state diffusive fluxes through bentonite using five different approaches.

Approach	Cl^- flux min mol/(m² · s)	Cl^- flux mol/(m² · s)	Cl^- flux max mol/(m² · s)
1 – Multiporosity	9.21E−14	1.21E−13	1.58E−13
2 – Van Loon et al.	1.69E−14	7.46E−14	1.32E−13
3 – Donnan	4.80E−14	6.99E−14	1.07E−13
4 – Ochs and Talerico	8.57E−15	2.86E−14	8.57E−14
5 – Wersin et al.	7.96E−15	2.20E−14	7.24E−14

Table 4-2. Parameters used in Idiart and Pękala (2016) to obtain steady-state diffusive fluxes through bentonite.

Parameter	Symbol	Value	Unit
Bentonite width	B_w	0.35	m
Ionic strength	I	0.24	−
Temperature	T	25	°C
External surface area of charged mineral	A_{ext}	45 000	m²/kg
Montmorillonite weight fraction	w_{mm}	0.75	−
Cl^- concentration ratio between EDL and free water	r	0.522	−

An additional verification of the multi-porosity model implementation in Comsol (approach 1) was performed with an equivalent model in Phreeqc. For that purpose, a 1D model was implemented in Phreeqc with a domain length of 0.35 m and a background NaCl concentration of 0.24 M. The EDL porosity was included by adding 0.361 sites/L_{water} of a negatively charged surface species, using the *Donnan* option available in Phreeqc (Parkhurst and Appelo 2013) and a Debye length multiplier of 2. The diffusion of a negatively charged tracer was studied with an initial concentration of 0 and imposing a concentration of 10^{-6} mol/L on the left boundary and 0 on the right boundary.

An equivalent model was simulated with Comsol, using the parameters given in Table 4-3. The total and interlayer porosities and pore diffusion coefficient were obtained with the methodology explained in Section 2.1. The ratio between EDL and free porewaters and the tracer concentrations (r) coincide with the values obtained with Phreeqc.

The results obtained with the two models in terms of EDL, free porosity, and average tracer concentrations are compared in Figure 4-1, showing a very good agreement.

Table 4-3. Parameters used in the Comsol multi-porosity verification model.

Parameter	Symbol	Value	Unit
Total porosity	ϕ_{tot}	0.42	–
Interlayer porosity	ϕ_{IL}	0.233	–
EDL porosity	ϕ_{EDL}	0.0294	–
Free porosity	ϕ_f	0.158	–
Tracer concentration ratio between EDL and free water	r	0.105	–
Pore diffusion coefficient	D_c	2.03×10^{-10}	m^2/s

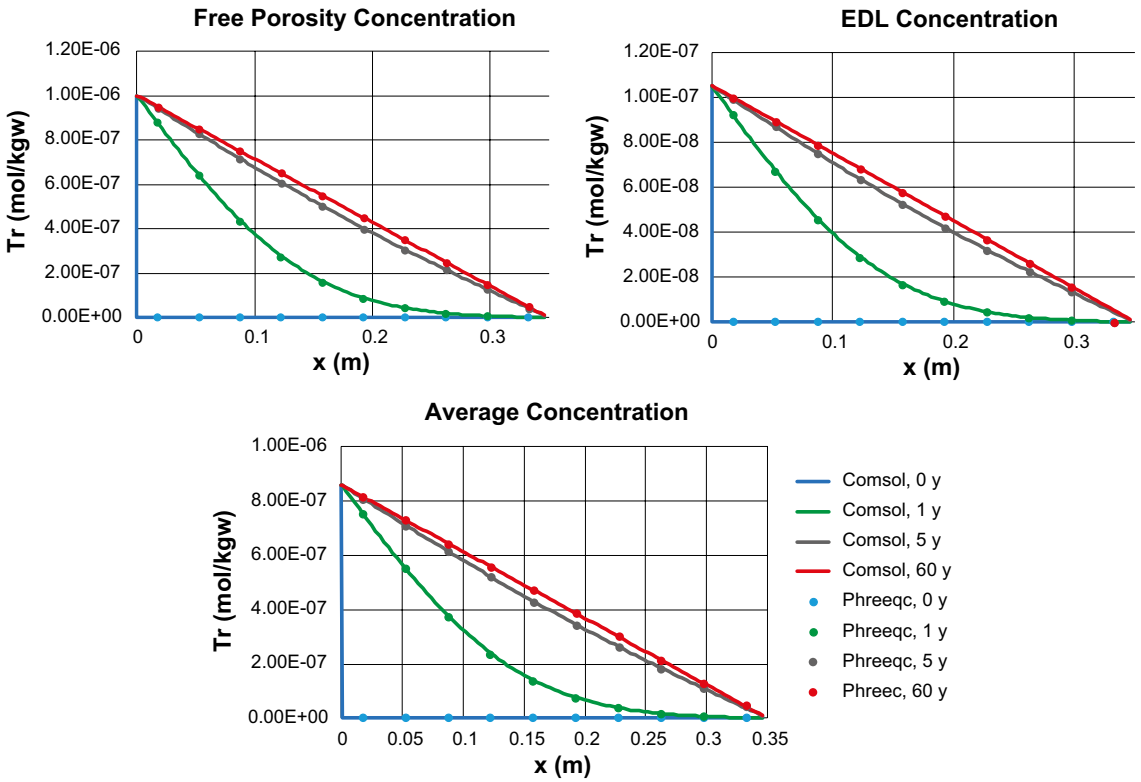

Figure 4-1. *Comparison between multi-porosity verification model results obtained with Comsol and PhreeqC.*

5 Numerical model setup

The conceptual model described in Chapter 3 is implemented as a two-dimensional (2D) radionuclide transport model using Comsol Multiphysics version 5.3 (COMSOL 2017) and its built-in physics *Transport of Diluted species in Porous Media*. The details of the numerical implementation are presented here.

The geometry represents a 1.82-meter-thick waste domain and 2.3-meter-thick bentonite backfill, both with a length of 15 m. The fractures intersecting the backfill are represented with a 0.5-mm-long edge (half the fracture aperture, for symmetry reasons) located at the lower part of the right bentonite boundary.

The finite element mesh used in the simulations is shown in Figure 5-1 and consists of 3 339 triangular elements. The maximum element size is 0.8 m, with a mesh refinement of 0.1 m at the bentonite-waste interface and of 1.0×10^{-4} m (0.1 mm) at the bentonite-fracture interface. This mesh was obtained by refining the aforementioned interfaces until reaching convergence of the $^{36}Cl^-$ release rates.

The boundary conditions are fixed concentration at the fracture boundary (Dirichlet boundary condition) and no concentration gradient (i.e. a no-flux boundary condition) at the contact with intact host rock and symmetry planes. In the sensitivity case that considers an equivalent fracture flow (Section 3.2.4), the Dirichlet boundary condition at the fracture boundary is replaced by a mass flux boundary condition (N_{36Cl} is imposed).

All simulations are carried out for a total time of 100 million years, imposing an absolute tolerance of the scaled $^{36}Cl^-$ concentration of 10^{-6} and a relative tolerance of 10^{-3} (COMSOL 2017).

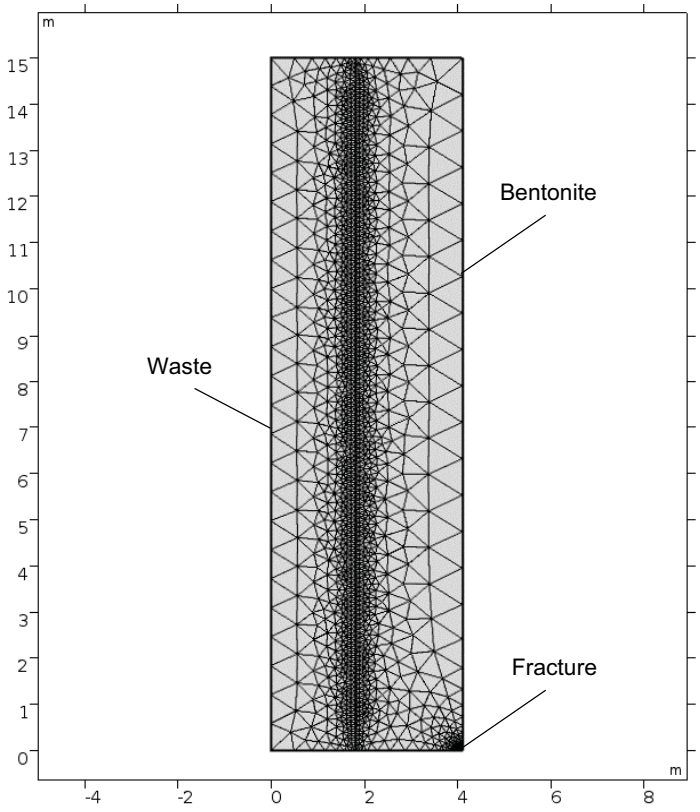

Figure 5-1. *Finite element mesh used in the radionuclide transport simulations. Dimensions expressed in meters.*

6 Results

The results of the 2D simulations of $^{36}Cl^-$ diffusion through bentonite are presented as: main transport parameters ($\phi_{av}D_e$) obtained with each model and temporal evolution of $^{36}Cl^-$ concentration (at specific points) and of total $^{36}Cl^-$ release from the BHA vault. The maximum $^{36}Cl^-$ fluxes in each approach, and the time at which these values are attained, are also given for all simulation cases. The results of the base case are presented first, followed by the main outcomes of the sensitivity cases and a final comparison.

6.1 Base case

The available porosities and effective diffusion coefficients obtained for the base case setup with the different methodologies described in Chapter 2 are summarized in Table 6-1. The available porosity values range between 11 % and 100 % of the total porosity ($\phi_t = 0.423$), whereas the effective diffusion coefficient values range between 2.70×10^{-12} and 5.33×10^{-11} m^2/s.

Figure 6-1 displays the evolution of $^{36}Cl^-$ concentration at the bentonite-waste interface and at the bentonite-host rock interface (specifically, at the mid-distance between two fractures) obtained with the different modelling approaches. The different approaches differ in how they model the transport of anions, in this case $^{36}Cl^-$, through compacted bentonite. Approaches 2 (Van Loon et al.), 4 (Ochs and Talerico) and 5 (Wersin et al.) model anion diffusion by reducing the available porosity and effective diffusion coefficients based on empirical or semi-empirical data, as can be seen in Table 6-1.

On the other hand, the Donnan equilibrium model (approach 3) reduces the anion concentration at the boundary with the external solution and thus the concentration gradients in the bentonite. The available porosity and effective diffusion coefficient of approach 3 are significantly higher as compared to the other approaches (Table 6-1), but still the concentrations of $^{36}Cl^-$ at the outlet are lower (see Figure 6-1). This is due to the effect of surface charge of the bentonite on the electrostatic potential gradient between the waste porewater and bentonite.

The multi-porosity model (approach 1) results in reduced anion diffusion due to a combination of two factors. Firstly, it accounts for a reduced available porosity based on anion exclusion from the interlayer porewater (Table 6-1). Note that the effective diffusion coefficient is lower than that of approach 3 (Donnan) and higher than that of the approaches based on empirical data. Secondly, the anion diffusion through bentonite is also slowed down in this approach due to reduced anion concentrations in the double layer (Figure 6-1).

Table 6-1. Available porosity and effective diffusion coefficient values obtained with the different base case models.

Approach	$\phi_{av,Cl}$ (-)	$\phi_{av,Cl}/\phi_t$ (-)	$D_{e,Cl}$ (m^2/s)
1 – Multiporosity	0.161	0.381	3.27×10^{-11}
2 – Van Loon et al.	0.045	0.106	5.52×10^{-12}
3 – Donnan	0.423	1.000	5.33×10^{-11}
4 – Ochs and Talerico	0.170	0.402	1.00×10^{-11}
5 – Wersin et al.	0.104	0.246	2.70×10^{-12}

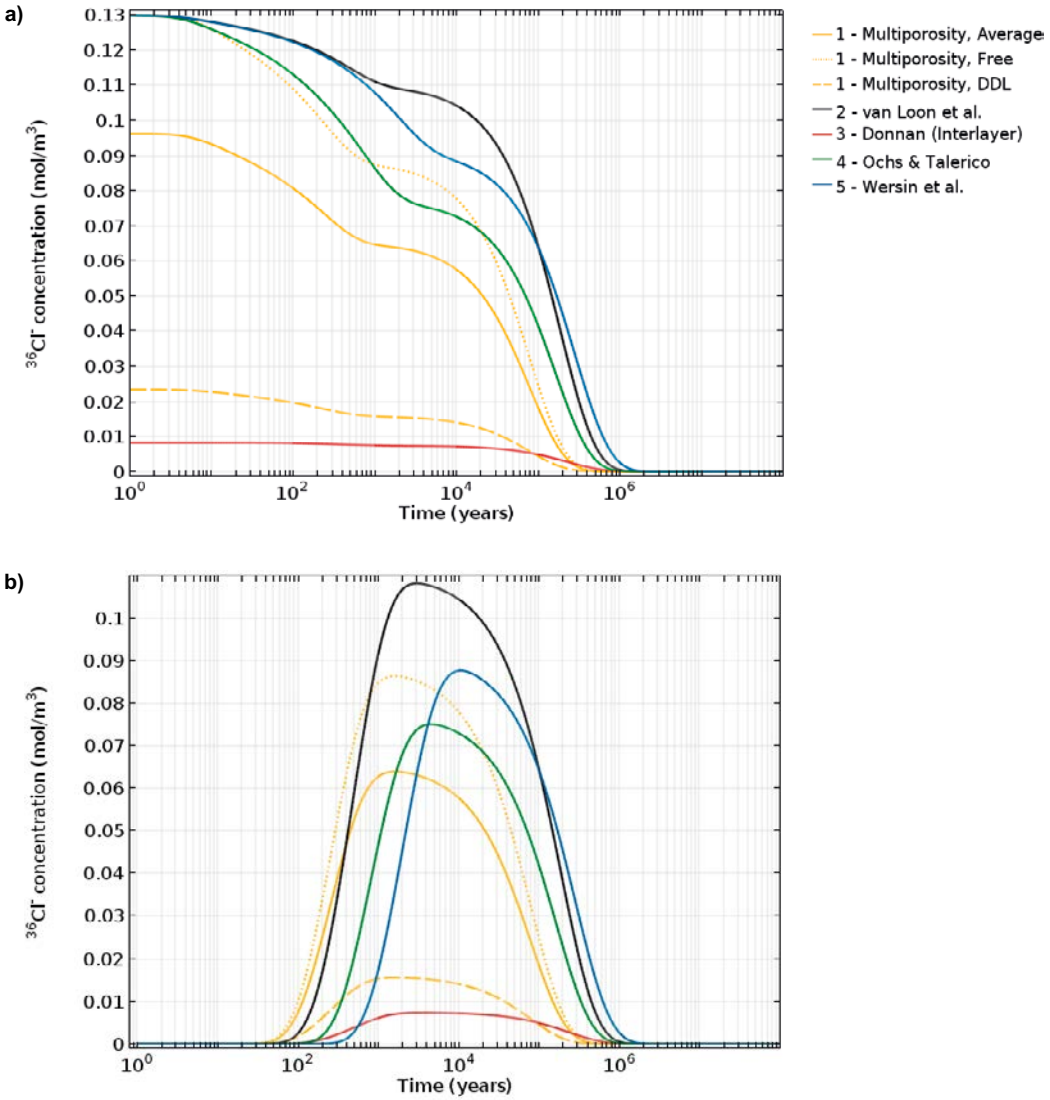

Figure 6-1. *Evolution of the $^{36}Cl^-$ concentration at a) the bentonite-waste interface and b) the bentonite-host rock interface at the mid-distance between two fractures.*

$^{36}Cl^-$ losses in the waste and bentonite domains occur due to two processes: diffusive release through the intersecting fractures and radioactive decay. The $^{36}Cl^-$ flux from the 2D bentonite domain into the fracture, in Bq/(s · m), has been calculated by integrating the flux through the bentonite-fracture interface as:

$$F_D = \frac{N_A \cdot \ln(2)}{t_{1/2}} \int_0^{\frac{a}{2}} -D_e \cdot \nabla c_{36Cl} \; dy \qquad \text{Equation 6-1}$$

where N_A is the Avogadro number (6.02×10^{23}), $t½$ the half-life of $^{36}Cl^-$ (9.49×10^{12} s), and a the fracture width (10^{-3} m). Note that F_D is the flux that corresponds to the 2D, 15m-long geometry described in Section 3.1. The total $^{36}Cl^-$ release of the entire BHA vault, in Bq/s, is then calculated as:

$$F_{BHA} = \frac{A_B}{W_B} \cdot \frac{L_{BHA}}{L_D} \cdot F_D \qquad \text{Equation 6-2}$$

A_B being the cross-section surface of the bentonite backfill (170.48 m^2, see Section 3.1.1), W_B the width of the bentonite domain in the 2D model (2.3 m), L_{BHA} the length of the BHA vault (140 m) and L_D the length of the 2D domain (15 m).

The $^{36}Cl^-$ loss of the waste and bentonite domains due to radioactive decay, in Bq/(m · s), is in turn calculated as follows:

$$D_D = \int_0^{L_D} \int_0^{W_w+W_B} \phi_{av,Cl}\, \lambda_{36Cl}\, c_{36Cl}\; dx\, dy \qquad \text{Equation 6-3}$$

where W_W is the width of the waste domain (1.813 m, see Section 3.1.1). Similarly, the total $^{36}Cl^-$ decay of the entire BHA vault, in Bq/s, is given by:

$$D_{BHA} = \frac{A_B}{W_B} \cdot \frac{L_{BHA}}{L_D} \cdot D_D \qquad \text{Equation 6-4}$$

Thus, the fraction of the total $^{36}Cl^-$ loss due to radioactive decay at a given time can be obtained with the following expression:

$$D_f = \frac{D_{BHA}}{D_{BHA} + F_{BHA}} = \frac{D_D}{D_D + F_D} \qquad \text{Equation 6-5}$$

Figure 6-2 displays the time evolution of total $^{36}Cl^-$ release from the BHA vault for each modelling approach. The maximum fluxes given in this figure, and the time at which they are reached, are summarized in Table 6-2. In general, three distinct phases are identified in the $^{36}Cl^-$ release from the BHA vault. During the first 1 000 to 5 000 years, depending on the model, the bentonite fills up with $^{36}Cl^-$ and the fluxes at the outlet gradually increase with time. Once the bentonite has reached high $^{36}Cl^-$ concentrations, a second phase with high release rates is maintained until around 1 million (10^6) years. Finally, in the third phase the $^{36}Cl^-$ mass flux drops with time as the concentration of $^{36}Cl^-$ in the waste domain decreases to very low values (Figure 6-1a).

Table 6-2. Maximum $^{36}Cl^-$ flux exiting the BHA vault, in Bq/year, obtained with each base case model and time at which this value is attained.

Approach	Maximum $^{36}Cl^-$ flux (Bq/year)	Time of maximum $^{36}Cl^-$ flux (years)
1 – Multiporosity	3.35E+08	1300
2 – Van Loon et al.	9.75E+07	2800
3 – Donnan	6.76E+07	2800
4 – Ochs and Talerico	1.23E+08	3900
5 – Wersin et al.	3.84E+07	9600

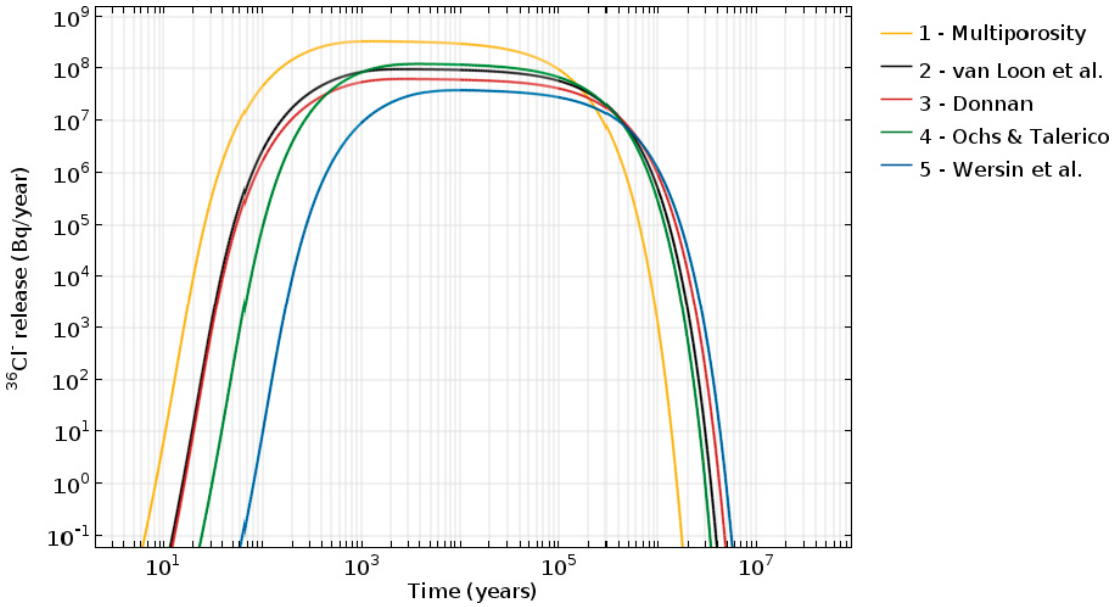

Figure 6-2. *Evolution of the total $^{36}Cl^-$ release from the BHA vault, in Bq/year, obtained with different modelling approaches of the base case.*

The different models yield comparable results and predict a maximum $^{36}Cl^-$ release of between 4×10^7 and 33×10^7 Bq/year. The multi-porosity model predicts the fastest release with a maximum $^{36}Cl^-$ flux of 3.35×10^8 Bq/year due to its high diffusion coefficient. The Donnan equilibrium model has an even higher diffusion coefficient, but $^{36}Cl^-$ fluxes obtained with this model are lower due to its lower concentration gradients (see Figure 6-1). The combined effect of the high diffusion coefficient and the low concentration gradients obtained with this approach (see Table 6-1 and Figure 6-1) results in release rates comparable to those obtained with other models, i.e. approaches 2 (Van Loon et al.) and 4 (Ochs and Talerico).

Approaches 2 (Van Loon et al.) and 4 (Ochs and Talerico) predict maximum $^{36}Cl^-$ release rates of around 1×10^8 Bq/year (Figure 6-2 and Table 6-2). As can be inferred from Figure 6-1, the $^{36}Cl^-$ concentration in bentonite increases slower for approach 4 (Ochs and Talerico) due to the higher available porosity accounted for in this model, which has a buffering effect.

Finally, Approach 5 (Wersin et al.) predicts the slowest release due to its low diffusion coefficient, with a maximum of 3.87×10^7 Bq/year. It is noted that this model is suitable for general anion diffusion through compacted bentonite and is not specific for $^{36}Cl^-$.

Figure 6-3 displays the time evolution of total radioactive decay of $^{36}Cl^-$ in the BHA vault (Figure 6-3a) and of the fraction of the total $^{36}Cl^-$ loss due to radioactive decay (Figure 6-3b). It can be seen that during the first 100 years approximately, the high $^{36}Cl^-$ concentrations and low fluxes cause that the vast majority of $^{36}Cl^-$ loss is due to radioactive decay. When $^{36}Cl^-$ fluxes increase, the radioactive decay fraction of the total loss drops towards an almost constant value, but is still significant in the long term in all modelling cases. Table 6-3 gives the accumulated fraction of initial $^{36}Cl^-$ loss due to decay and release at different times. It can be seen that in the case with the fastest release, i.e. using approach 1 (multiporosity), the decay fraction reaches a final value of 18.5 %, while for the case with the slowest release, i.e. using approach 5 (Wersin et al.), radioactive decay constitutes as much as 65.9 % of the total $^{36}Cl^-$ loss.

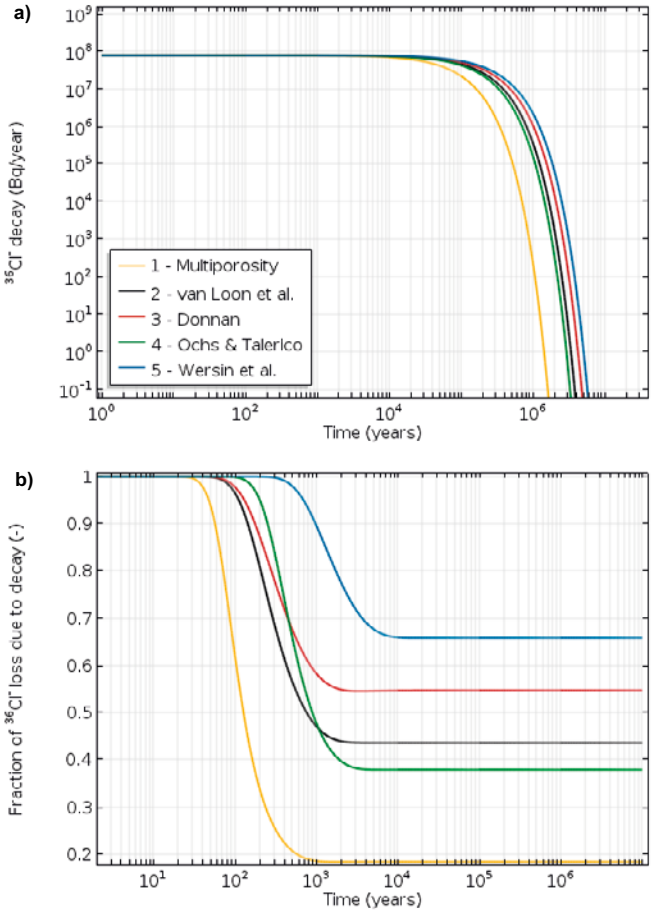

Figure 6-3. *Evolution in time of a) the total radioactive $^{36}Cl^-$ decay in the BHA vault (waste + bentonite), in Bq/year, and b) the fraction of total $^{36}Cl^-$ loss due to radioactive decay, obtained with different modelling approaches of the base case.*

Table 6-3. Cumulative fraction (-) of initial $^{36}Cl^-$ loss due to release and decay at different times obtained with the different modelling approaches applied to the base case.

Time (years)	Approach 1 – Multiporosity		Approach 2 – van Loon et al.		Approach 3 – Donnan		Approach 4 – Ochs and Talerico		Approach 5 – Wersin et al.	
	Release	Decay	Release	Decay	Release	Decay	Release	Decay	Release	Decay
10^5	0.581	0.132	0.230	0.179	0.155	0.188	0.280	0.173	0.099	0.195
10^6	0.815	0.185	0.560	0.434	0.446	0.538	0.618	0.379	0.330	0.639
10^7	0.815	0.185	0.563	0.436	0.453	0.547	0.620	0.380	0.340	0.659

6.2 Sensitivity cases

6.2.1 Effect of homogeneous background electrolyte composition

The sensitivity of the models to the background chemistry used for the bentonite domain was tested with three porewaters that differ in salinity (Section 3.2.1). The base case composition, which corresponds to a bentonite porewater, has an ionic strength of 0.227 M, while the saline, old meteoric, and glacial porewaters tested here have ionic strengths of 1.628, 7×10^{-3} and 5×10^{-5} M, respectively.

Approach 1 (Multiporosity) was tested with the saline porewater only, apart from the base case, as low salinities result in negative free porosities. In this model, the ionic strength of the porewater solution affects how the available porosity is distributed between double layer and free porosities and the concentration ratio of chloride in these porosities, see Table 6-4. A higher salinity results in smaller double layer porosities and larger free porosities, and thus higher $^{36}Cl^-$ concentrations. The overall result of this is a higher average $^{36}Cl^-$ concentration in the bentonite when considering a saline solution (see Figure 6-4), and a slight increase in $^{36}Cl^-$ release rates from the BHA vault (see Figure 6-5 and Table 6-6).

Table 6-4. Available, double layer and free porosities and Cl^- concentration ratio between EDL and free water values obtained with approach 1 (multi-porosity model) using different porewater compositions in bentonite.

Simulation case	$\phi_{av,Cl}$ (-)	ϕ_{EDL} (-)	ϕ_f (-)	r (-)
Base case	0.161	0.051	0.110	0.180
Saline	0.161	0.019	0.142	0.371

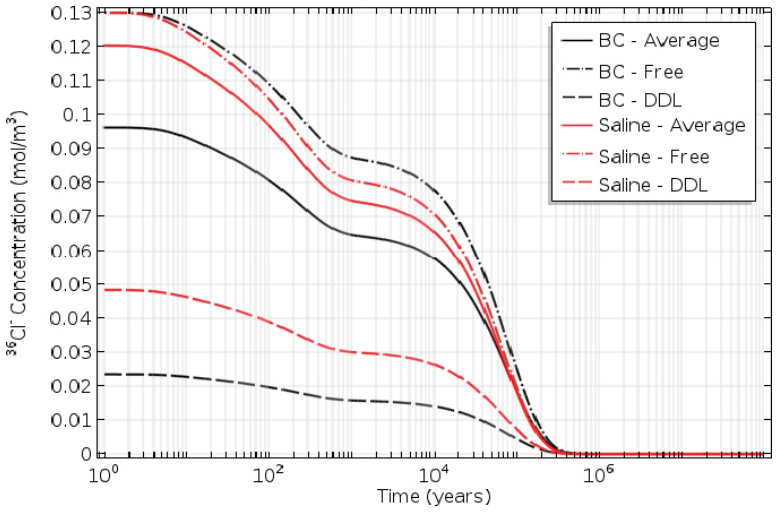

Figure 6-4. Evolution of the $^{36}Cl^-$ concentrations used in approach 1 (multi-porosity model) at the bentonite-waste interface using bentonite porewater (black lines) and saline groundwater (red lines) compositions in the bentonite.

Approach 2 (Van Loon et al.) was tested with all pore solutions described above. In this model, the ionic strength of the background solution affects the porosity available to chloride ions (Equation 2-16) and the diffusion coefficient through bentonite (Equation 2-17). The values obtained for these variables with each of the background solutions are given in Table 6-5. The results of the sensitivity study, in terms of $^{36}Cl^-$, are given in Figure 6-5 and Table 6-6. The saline solution causes an increase of the radionuclide release rates by a factor of 3, while the solutions with low salinity decrease them by almost two orders of magnitude. Due to the exponential relation between $\phi_{av,Cl}$ and I, reducing the ionic strength of the solution does not have a large effect on radionuclide release for very low salinities.

The sensitivity study of approach 5 (Wersin et al.) to bentonite background solutions was restricted to the saline groundwater, as the old meteoric and glacial porewaters lead to negative accessible porosities. The high ionic strength of the saline solution results in a higher available porosity and diffusion coefficient, see Equations 2-24–2-28, as can be observed in Table 6-5. Also, in this approach the use of a saline solution results in a $^{36}Cl^-$ flux increase by a factor of 3, see Figure 6-5 and Table 6-6.

Table 6-5. Available porosity and effective diffusion coefficient values obtained with approaches 2 (Van Loon et al.) and 5 (Wersin et al.) using different porewater compositions in bentonite.

Approach	Simulation case	$\phi_{av,Cl}$ (-)	$D_{e,Cl}$ (m²/s)
2 – Van Loon et al.	Base case	0.045	5.52×10^{-12}
	Saline	0.096	2.37×10^{-11}
	Meteoric	0.0075	1.88×10^{-13}
	Glacial	0.0060	1.22×10^{-13}
5 – Wersin et al.	Base case	0.104	2.70×10^{-12}
	Saline	0.171	9.54×10^{-12}

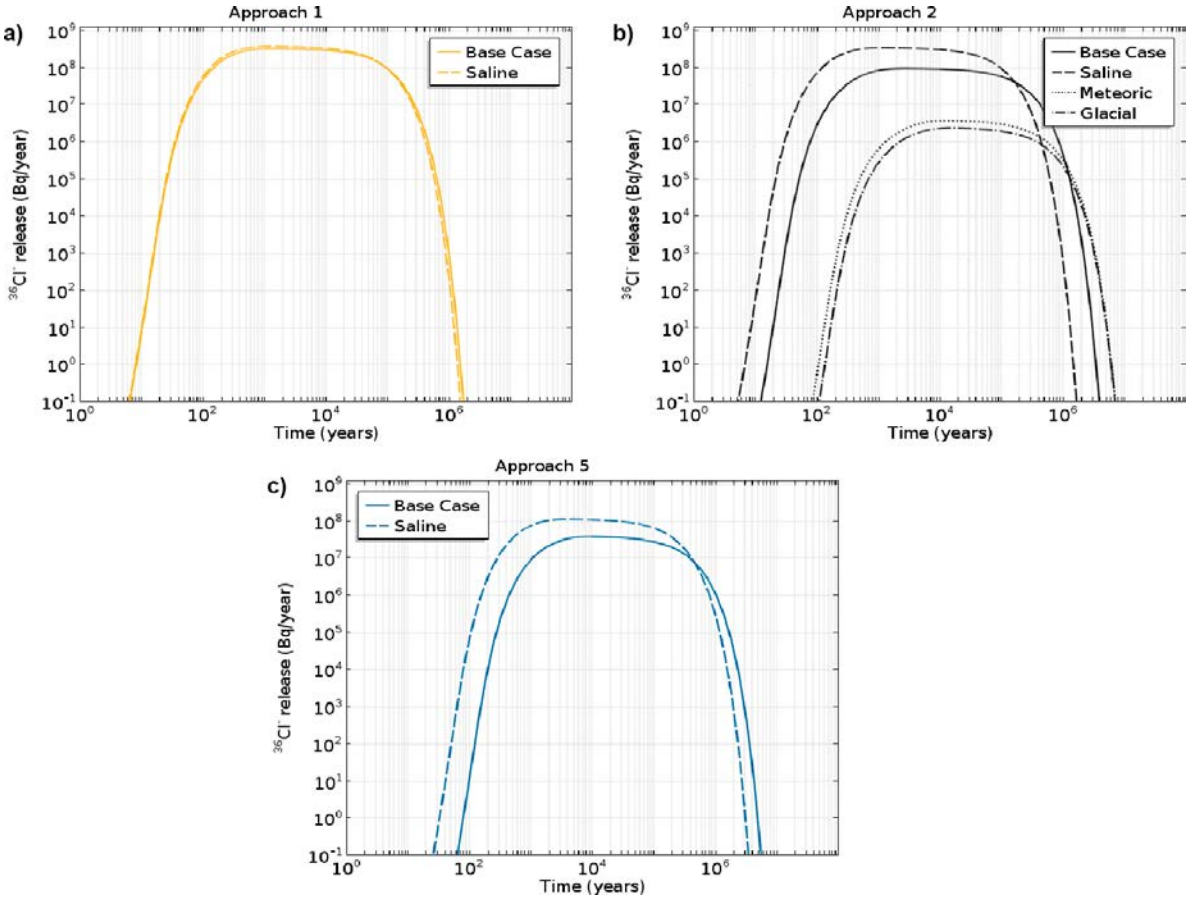

Figure 6-5. *Evolution of the total $^{36}Cl^-$ release from the BHA vault, in Bq/year, obtained with approaches 1 (multi-porosity) (a), 2 (Van Loon et al.) (b), and 5 (Wersin et al.) (c) using different porewater compositions in bentonite.*

6.2.2 Effect of space-dependent background electrolyte composition

Approach 2 (Van Loon et al. 2007) is also used to assess the effect of considering a space-dependent background electrolyte composition. This heterogeneous composition corresponds to a steady-state situation in which the waste domain has a fixed concrete porewater composition and the fracture a porewater composition corresponding to meteoric groundwater. The effective diffusion coefficient and chloride accessible porosity of bentonite obtained with this setup are given in Figure 6-6. Both variables present lower values than the base case, in general, and values as low as the old meteoric sensitivity case in a small region close to the fracture.

The $^{36}Cl^-$ fluxes obtained with this sensitivity case are given in Figure 6-7 and Table 6-6. The heterogenous background composition yields release rates that are one order of magnitude smaller than in the base case.

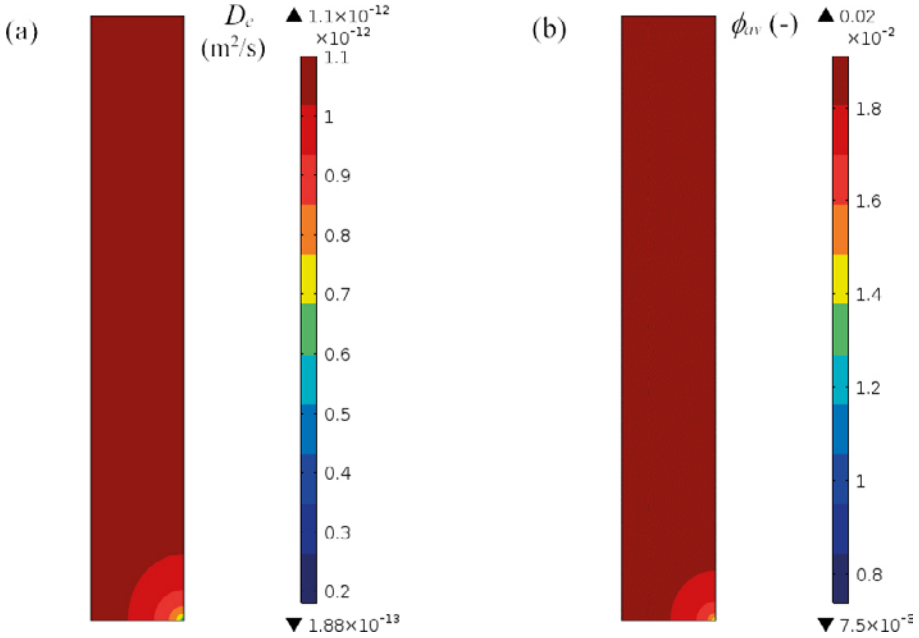

Figure 6-6. *Spatial distribution of (a) effective diffusion coefficient (m^2/s) and (b)chloride available porosity obtained for the bentonite domain using approach 2 (Van Loon et al.) and a heterogenous porewater composition.*

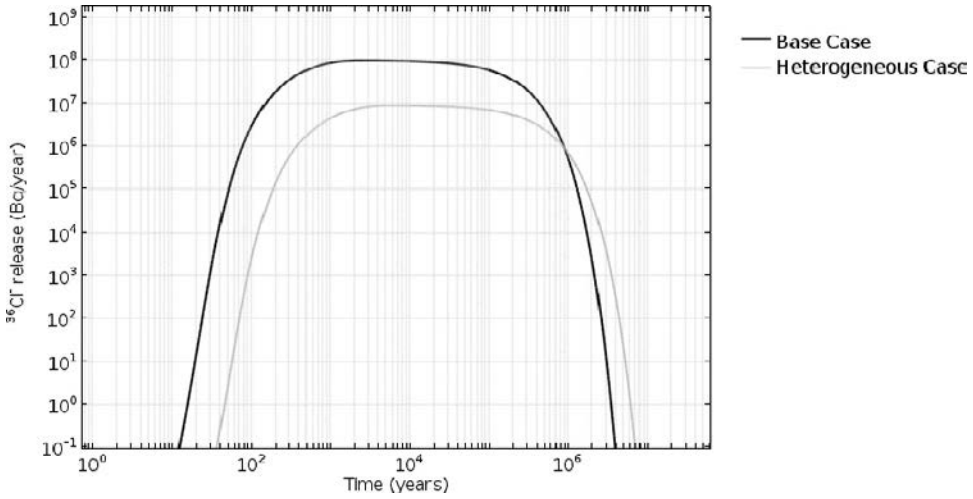

Figure 6-7. *Evolution of the total $^{36}Cl^-$ release from the BHA vault, in Bq/year, obtained with approach 2 (Van Loon et al.) using a bentonite porewater composition (black line), and a heterogenous porewater composition (grey line) in the bentonite domain.*

6.2.3 Effect of diffusion coefficient of bentonite

The sensitivity of the different models to the effective diffusion coefficient was tested by increasing and decreasing the base case value by a factor of 10. The resulting $^{36}Cl^-$ release fluxes are given in Table 6-6.

Varying the diffusion coefficient has a similar effect on all models. In general, the fluxes reflect the variation of the diffusion coefficient. There is an effect of the radioactive decay of $^{36}Cl^-$, however, which becomes more important in those cases that present lower release rates. In approach 1 (multi-porosity model), the effect of radioactive decay is limited (see Figure 6-3), and the peak flux and the time of the peak flux scale linearly with the diffusion coefficient. In approach 5 (Wersin et al.), on the other hand, radioactive decay constitutes a big contribution to $^{36}Cl^-$ concentration decrease in the vault due to its relatively low release rates. For that reason, varying the diffusion coefficient does not have a linear effect on the release rates of this approach. As can be seen in Table 6-5, the maximum flux in the base case is 3.84×10^7 Bq/year. Increasing the diffusion coefficient by a factor of 10 causes a release rate that is 10.3 times higher (3.95×10^8 Bq/year) due to a reduction in $^{36}Cl^-$ decay. The opposite case, i.e. a diffusion coefficient decrease by a factor of 10, causes a release rate decrease by a factor of 11.5 (3.34×10^6 Bq/year) due to an increased effect of $^{36}Cl^-$ decay.

6.2.4 Effect of equivalent fracture flow, Q_{eq}

The impact of modelling the fractures in the host rock with an equivalent flow, Q_{eq}, instead of as perfect sinks, is assessed with approaches 2 (Van Loon et al.), 4 (Ochs and Talerico), and 5 (Wersin et al.). Limiting the transport capacity of the fractures with an equivalent flow results in $^{36}Cl^-$ concentrations that are generally greater than zero at the interface between the bentonite and the fractures (see Figure 6-8).

The results obtained with the equivalent fracture flow approximation are compared to the base case results in Figure 6-9 and Table 6-6. In all studied cases, using an equivalent fracture flow restricts the radionuclide release to some extent as compared to the base case (between 7 and 20 %). It can also be concluded that the impact of the limited fracture transport capacity is larger the higher the diffusive fluxes.

The results obtained with the simplified model of Wessely and Shahkarami (2019), displayed in Figure 6-9, were obtained with parameter values given by Ochs and Talerico (2004), which are very similar to those of approach 4 (Ochs and Talerico), and using the same Q_{eq} as in this sensitivity case. The fluxes predicted by approach 4 (Ochs and Talerico) and Wessely and Shahkarami (2019) are found to be in reasonably good agreement despite the fact that the modelling setups (numerical approach, geometry, spatial and time discretization, etc.) are quite different.

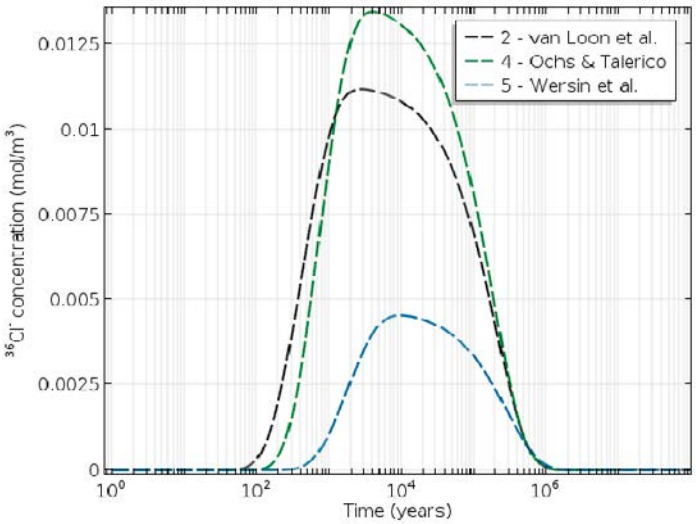

Figure 6-8. *Evolution of the $^{36}Cl^-$ concentration at the bentonite-fracture interface obtained with approaches 2 – Van Loon et al. (black), 4 – Ochs and Talerico (green) and 5 – Wersin et al. (blue) using an equivalent fracture flow.*

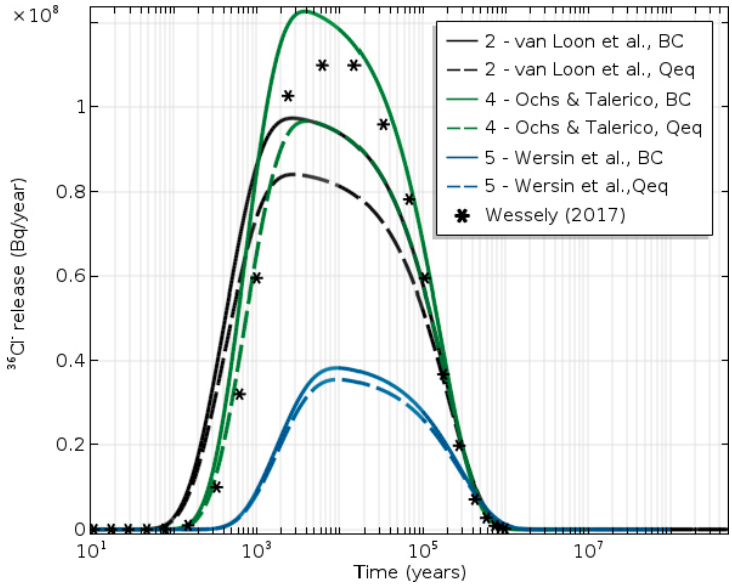

Figure 6-9. *Evolution of the $^{36}Cl^-$ release from the BHA vault, in Bq/year, obtained with approaches 2 – Van Loon et al. (black lines), 4 – Ochs and Talerico (green lines) and 5 – Wersin et al. (blue lines) modelling the fractures as perfect sinks (full lines) and with an equivalent fracture flow (dashed lines), and comparison with the results from Wessely and Shahkarami (2019) obtained using a simplified model (black stars).*

6.3 Summary of results

A summary of the maximum $^{36}Cl^-$ release of all modelled cases is given in Table 6-6.

Table 6-6. Maximum $^{36}Cl^-$ flux released from the BHA vault, in Bq/year, obtained with each model, and time at which this value is attained.

Approach	Simulation case	Maximum $^{36}Cl^-$ flux (Bq/year)	Time of maximum $^{36}Cl^-$ flux (years)
1 – Multiporosity	Base case	3.35E+08	1 300
	Saline	3.87E+08	1 200
	Low $D_{e,Cl}$	3.32E+07	11 000
	High $D_{e,Cl}$	3.35E+09	140
2 – Van Loon et al.	Base case	9.75E+07	2 800
	Saline	3.51E+08	1 200
	Meteoric	3.66E+06	13 000
	Glacial	2.39E+06	16 000
	Heterogeneous	8.63E+06	6 500
	Low $D_{e,Cl}$	9.30E+06	21 000
	High $D_{e,Cl}$	9.74E+08	280
	Q_{eq}	8.41E+07	2 800
3 – Donnan	Base case	6.32E+07	2 800
	Low $D_{e,Cl}$	6.03E+06	21 000
	High $D_{e,Cl}$	6.23E+08	390
4 – Ochs and Talerico	Base case	1.23E+08	3 900
	Low $D_{e,Cl}$	1.14E+07	38 000
	High $D_{e,Cl}$	1.23E+09	390
	Q_{eq}	9.68E+07	4 100
5 – Wersin et al.	Base case	3.84E+07	9 600
	Saline	1.15E+08	4 100
	Low $D_{e,Cl}$	3.34E+06	62 000
	High $D_{e,Cl}$	3.95E+08	1 100
	Q_{eq}	3.56E+07	9 700

7 Summary and conclusions

SKB plans to dispose of long-lived low and intermediate level waste in the SFL repository, in which the BHA vault relies on a bentonite backfill for radionuclide confinement. It is generally accepted that solute transport in water saturated bentonite is dominated by diffusion, but the mechanistic description of this process is not as well-established. In this work, five different models for anion diffusion in compacted bentonite have been used to estimate the long-term release of $^{36}Cl^-$ radionuclides from the BHA vault, as well as to quantify the variability induced by using different modelling approaches. Two of these models are empirical, one is semi-empirical and the other two are mechanistic. They differ in the chloride accessible porosity they take into account, the effective diffusion coefficient of bentonite and the chemical equilibrium between bentonite and external porewaters. All models are implemented in Comsol Multiphysics version 5.3 (COMSOL 2017) and consider a 2D geometry of the BHA vault.

A base case has been formulated that considers expected repository conditions. The different simulations predict a maximum $^{36}Cl^-$ release of $4–33 \times 10^7$ Bq/year reached after 1 300–9 600 years. In general, the different modelling approaches yield comparable results except for the multi-porosity model, which yields a flux that is 3 – 4 times higher than the rest (see Figure 7-1). It should be noted that the results obtained with the multi-porosity model (approach 1) depend on the values of several parameters that have not been adjusted using experimental data and therefore are subject to uncertainties (see Table 3-1). Therefore, it is likely that the reason why this model over-predicts $^{36}Cl^-$ fluxes is because of a lack of a detailed description of these parameters. Approaches 2-5 simplify the porosity microstructure of bentonite in different ways, but probably produce more realistic results because the few parameters used in these models have been adjusted to experimental data. The most reliable base case results are considered to be those produced by approach 4 (Ochs and Talerico). This is because the parameters of this model have been obtained specifically for chloride diffusion through bentonite under repository conditions. However, it is noted that this approach is not sensitive to the ionic strength of the background solution.

Additionally, a set of sensitivity analyses was performed in order to assess the impact of bentonite porewater composition, its effective diffusion coefficient, and the magnitude of the equivalent flow through the fractures intersecting the vault.

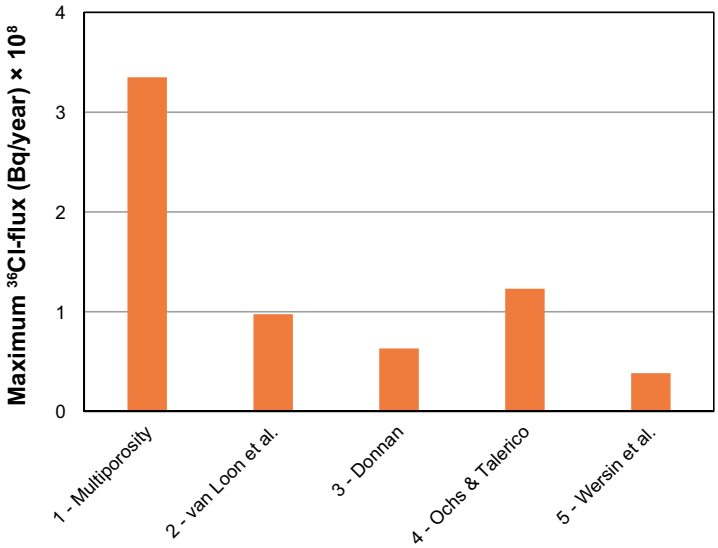

Figure 7-1. *Maximum $^{36}Cl^-$ fluxes obtained for the base case setup using the different modelling approaches.*

The results indicate that saline solutions in the bentonite lead to higher anion accessible porosities and thus accelerate $^{36}Cl^-$ release. Solutions with low ionic strength, on the other hand, slow down the release, but only to a certain extent. This indicates that it is important to estimate $^{36}Cl^-$ release from the BHA vault with realistic background electrolyte compositions. Also, in cases in which ionic strength differs significantly from the base Case value of this work it would be recommendable to predict $^{36}Cl^-$ release with approach 2 (Van Loon et al.), which compares well with approach 4 (Wersin et al.) in the base case, is sensitive to the ionic strength, and is also straightforward to implement.

It was also observed that varying the effective diffusion coefficient in a given model has a direct impact on the $^{36}Cl^-$ fluxes leaving the bentonite, with a small effect of radionuclide decay. Furthermore, modelling the host-rock fractures with an equivalent flow approach (Q_{eq}) instead of as a perfect sink slightly reduces the radionuclide release (by 7–20 %), especially in cases with high diffusion coefficients in bentonite. This indicates that it is reasonable to simplify the model by considering fractures that act as prefect sinks, and that models with this simplification will overestimate $^{36}Cl^-$ fluxes and constitute a (slightly) conservative case.

References

SKB's (Svensk Kärnbränslehantering AB) publications can be found at www.skb.com/publications. SKBdoc documents will be submitted upon request to document@skb.se.

Appelo C A J, 2013. A review of porosity and diffusion in bentonite. Posiva Working Report 2013-29, Posiva Oy, Finland.

Appelo C A J, Postma D, 2005. Geochemistry, groundwater and pollution. 2nd ed. Leiden: Balkema.

Birgersson M, Karnland O, 2009. Ion equilibrium between montmorillonite interlayer space and an external solution – Consequences for diffusional transport. Geochimica et Cosmochimica Acta, 73, 1908–1923.

Bourg I C, Bourg A C M, Sposito G, 2003. Modeling diffusion and adsorption in compacted bentonite: a critical review. Journal of Contaminant Hydrology 61, 293–302.

Bradbury M H, Baeyens B, 2003. Porewater chemistry in compacted re-saturated MX-80 bentonite. Journal of Contaminant Hydrology 61, 329–338.

COMSOL, 2017. COMSOL Multiphysics® v. 5.3. COMSOL AB, Sweden.

Elfwing M, Evins L Z, Gontier M, Grahm P, Mårtensson P, Tunbrant S, 2013. SFL concept study. Main report. SKB TR-13-14, Svensk kärnbränslehantering AB.

Gimeno M J, Auqué L F, Gómez J B, Salas J, Molinero J, 2010. Hydrogeochemical evolution of the Laxemar site. SKB R-10-60, Svensk Kärnbränslehantering AB.

Hartley L, Hoch A, Jackson P, Joyce S, McCarthy R, Rodwell W, Swift B, Marsic N, 2006. Groundwater flow and transport modelling during the temperate period for the SR-Can assessment. Forsmark area – version 1.2. SKB R-06-98, Svensk Kärnbränslehantering AB.

Idiart A, Pękala M, 2016. Models for diffusion in compacted bentonite. SKB TR-15-06, Svensk Kärnbränslehantering AB.

Idiart A, Laviña M, Grandia F, 2019. Reactive transport modelling of montmorillonite dissolution. Report for the safety evaluation SE-SFL. SKB R-19-15, Svensk Kärnbränslehantering AB.

Muurinen A, Karnland O, Lehikoinen J, 2007. Effect of homogenization on the micro-structure and exclusion of chloride in compacted bentonite. Physics and Chemistry of the Earth, Parts A/B/C 32, 485–490.

Nardi A, Idiart A, Trinchero P, de Vries L M, Molinero J, 2014. Interface COMSOL-PHREEQC (iCP), an efficient numerical framework for the solution of coupled multiphysics and geochemistry. Computers & Geosciences 69, 10–21.

Ochs M, Talerico C, 2004. SR-Can. Data and uncertainty assessment. Migration parameters for the bentonite buffer in the KBS-3 concept. SKB TR-04-18, Svensk Kärnbränslehantering AB.

Parkhurst D L, Appelo C A J, 2013. Description of input and examples for PHREEQC version 3 – A computer program for speciation, batch-reaction, one-dimensional transport, and inverse geochemical calculations. Techniques and Methods 6–A43, U.S. Geological Survey, Denver, Colorado.

Pękala M, Olmeda J, Grivé M, Bruno J, 2015. Assessment of redox state and its impact on the solubility and speciation of selected radionuclides in the SFL repository. Final report. Amphos 21. SKBdoc 1533627 ver 1.0, Svensk Kärnbränslehantering AB.

Pusch R, 2001. The microstructure of MX-80 clay with respect to its bulk physical properties under different environmental conditions. SKB TR-01-08, Svensk Kärnbränslehantering AB.

SKB, 2006. Data report for the safety assessment SR-Can. SKB TR-06-25, Svensk Kärnbränslehantering AB.

SKB, 2010. Data report for the safety assessment SR-Site. SKB TR-10-52, Svensk Kärnbränslehantering AB.

SKB, 2011. Long-term safety for the final repository for spent nuclear fuel at Forsmark. Main report of the SR-Site project. SKB TR-11-01, Svensk Kärnbränslehantering AB.

SKB, 2019. Initial state for the repository for the safety evaluation SE-SFL. SKB TR-19-03, Svensk Kärnbränslehantering AB.

Tournassat C, 2008. A predictive model for anion exclusion in compacted Na-montmorillonite. In 4th Annual Workshop Proceedings 6th EC-FP-FUNMIG IP, Karlsruhe, November 2008, 123–142.

Van Loon L R, Glaus M A, Müller W, 2007. Anion exclusion effects in compacted bentonites: towards a better understanding of anion diffusion. Applied Geochemistry 22, 2536–2552.

Wersin P, 2003. Geochemical modelling of bentonite porewater in high-level waste repositories. Journal of Contaminant Hydrology 61, 405– 422.

Wersin P, Curti E, Appelo C A J, 2004. Modelling bentonite–water interactions at high solid/liquid ratios: swelling and diffuse double layer effects. Applied Clay Science 26, 249–257.

Wersin P, Kiczka M, Rosch D, 2014. Safety case for the disposal of spent nuclear fuel at Olkiluoto. Radionuclide solubility limits and migration parameters for the canister and buffer. Posiva 2012-39, Posiva Oy, Finland.

Wessely O, Shahkarami P, 2019. Development of radionuclide transport models for the near-field. Report for the safety evaluation SE-SFL. SKB R-19-05, Svensk Kärnbränslehantering AB.

Arkitektkopia AB, Bromma, 2019

SKB is responsible for managing spent nuclear fuel and radioactive waste produced by the Swedish nuclear power plants such that man and the environment are protected in the near and distant future.

skb.se